

Reconstructing the genealogy of LIGO-Virgo black holes

PARTHAPRATIM MAHAPATRA,¹ DEBATRI CHATTOPADHYAY,² ANURADHA GUPTA,³ FABIO ANTONINI,² MARC FAVATA,⁴
B. S. SATHYAPRAKASH,^{5,6,2} AND K. G. ARUN^{1,6}

¹*Chennai Mathematical Institute, Siruseri, 603103, India*

²*School of Physics and Astronomy, Cardiff University, Cardiff, CF24 3AA, United Kingdom*

³*Department of Physics and Astronomy, The University of Mississippi, University, Mississippi 38677, USA*

⁴*Department of Physics & Astronomy, Montclair State University, 1 Normal Avenue, Montclair, NJ 07043, USA*

⁵*Institute for Gravitation and the Cosmos, Department of Physics, Penn State University, University Park, PA 16802, USA*

⁶*Department of Astronomy and Astrophysics, Penn State University, University Park, PA 16802, USA*

(Dated: June 11, 2024)

ABSTRACT

We propose a Bayesian inference framework to predict the merger history of LIGO-Virgo binary black holes, whose binary components may have undergone hierarchical mergers in the past. The framework relies on numerical relativity predictions for the mass, spin, and kick velocity of the remnant black holes. This proposed framework computes the masses, spins, and kicks imparted to the remnant of the parent binaries, given the initial masses and spin magnitudes of the binary constituents. We validate our approach by performing an “injection study” based on a constructed sequence of hierarchically-formed binaries. Noise is added to the final binary in the sequence, and the parameters of the ‘parent’ and ‘grandparent’ binaries in the merger chain are then reconstructed. This method is then applied to three GWTC-3 events: GW190521, GW200220_061928, GW190426_190642. These events were selected because at least one of the binary companions lies in the putative pair-instability supernova mass gap, in which stellar processes alone cannot produce black holes. Hierarchical mergers offer a natural explanation for the formation of black holes in the pair-instability mass-gap. We use the backward evolution framework to predict the parameters of the parents of the primary companion of these three binaries. Our results indicate that at least one component of these three observed binaries was formed through a prior binary black hole merger. This approach can be readily applied to future high-mass gravitational wave events to predict their formation history under the hierarchical merger assumption.

Keywords: Stellar mass black hole, Gravitational Waves, Star clusters, Bayesian statistics

1. INTRODUCTION

Dense stellar environments such as globular clusters (GCs), nuclear star clusters (NSCs), or gaseous active galactic nuclei (AGN) disks are expected to contain large numbers of black holes (BHs). In such environments, the BH remnant formed from a binary black hole (BBH) merger could pair with another BH and subsequently merge. This process could repeat, leading to multiple generations of sequentially more massive BBHs—a phenomenon referred to as hierarchical mergers (Miller &

Hamilton 2002; O’Leary et al. 2006; Antonini & Rasio 2016; Gerosa & Berti 2017; Fragione et al. 2018; Banerjee 2018; Fishbach et al. 2017; Rodriguez et al. 2018; Antonini et al. 2019; Yang et al. 2019; Gerosa & Berti 2019; Fragione & Silk 2020; Mapelli et al. 2021; Britt et al. 2021; Kritos et al. 2022; Chattopadhyay et al. 2023; Antonini et al. 2023; Fragione & Rasio 2023). Since BBH mergers generically impart a gravitational kick (Fitchett 1983; Favata et al. 2004) to the remnant BHs that can be of the order of 1000 km/s, hierarchical mergers can only occur in astrophysical environments that have escape speeds large enough to retain the merger remnants (preferably $\gtrsim 200$ km/s (Mahapatra et al. 2021);

see also Merritt et al. (2004); Gerosa & Berti (2019); Doctor et al. (2021); Mahapatra et al. (2022)).

By analyzing the binary component masses and spin parameters, several studies (Yang et al. 2019; Kimball et al. 2020, 2021; Gerosa et al. 2020; Tagawa et al. 2020; Gupta et al. 2020; Tagawa et al. 2021; Rodriguez et al. 2020; Gerosa & Fishbach 2021; Baibhav et al. 2021; Liu & Lai 2021) have identified potential hierarchical merger candidates among the BBHs observed by LIGO/Virgo (Aasi et al. 2015; Acernese et al. 2014). GW190521 (Abbott et al. 2020a,b) is one such example as its massive primary might lie in the pair-instability supernova or pulsational pair-instability supernova mass-gap between $\sim 50M_{\odot}$ – $130M_{\odot}$ (Fowler & Hoyle 1964; Barkat et al. 1967; Heger et al. 2003; Woosley et al. 2007; Woosley 2017; Farmer et al. 2019; Renzo et al. 2020b,c; Marchant et al. 2019) (also referred to as the “upper mass gap”). In that mass region stellar processes are thought to be incapable of producing BHs, suggesting that BHs with such masses are possibly formed via dynamical interactions in dense star clusters or AGN discs. However, the precise range of the upper mass gap is sensitive to the uncertain nuclear reaction rates in the late evolution of massive stars (Farmer et al. 2020; Renzo et al. 2020c; Farmer et al. 2019; Marchant & Moriya 2020; Woosley & Heger 2021). Moreover, BHs formed from progenitor stars with very low metallicities ($Z \leq 0.0003$) might altogether avoid the mass limit imposed by pair instability (Costa et al. 2021; Farrell et al. 2021). This suggests that the formation of the most massive BHs thus far detected by LIGO/Virgo could be explained by either stellar processes (if the mass gap lies near the high mass end of current theoretical estimates) or by hierarchical BH mergers in dense clusters.¹ Some studies of the population properties of merging BBHs have reported evidence of a potential subpopulation of hierarchical mergers in the present data (Tiwari & Fairhurst 2021; Kimball et al. 2021; Baxter et al. 2021; Mould et al. 2022; Mahapatra et al. 2022), but more data is needed to reach a definitive conclusion (Abbott et al. 2023a; Fishbach et al. 2022).

¹ There are others mechanisms that can produce BHs in the upper mass gap, including envelope retention in metal-poor population III stars (Tanikawa et al. 2021; Kinugawa et al. 2021), the mergers of massive stars prior to compact binary formation in low-metallicity young star clusters (Di Carlo et al. 2020; Renzo et al. 2020a; Kremer et al. 2020; González et al. 2021), and accretion scenarios (Woosley & Heger 2021; van Son et al. 2020; Rice & Zhang 2021; Safarzadeh & Haiman 2020; Roupas & Kazanas 2019; Natarajan 2021). However, it is not clear how common these processes are in nature and if they can explain the rates of massive BH mergers such as GW190521.

Using the framework of Kimball et al. (2020), Abbott et al. (2020b) calculated the odds ratio that GW190521 is a hierarchical merger versus a 1g+1g merger. Abbott et al. (2020b) found that GW190521 is favored to be a 1g+1g merger over a 1g+2g merger with the odds ratio spanning the range 1:1 to 4:1 (depending on the waveform model and the population model). The odds ratio for a 1g+1g merger over a 2g+2g merger span the range 1:1 to 33:1. Both cases assume the merger occurred in a Milky Way type GC (escape speed $V_{\text{esc}} \approx 60$ km/s) (Rodriguez et al. 2019). However, the odds of GW190521 being of hierarchical origin increases by 3–4 orders of magnitude compared to the previous estimates if one considers clusters with $V_{\text{esc}} \approx 800$ km/s [which may be representative of NSCs (Abbott et al. 2020b)]. Later, Kimball et al. (2021) extended this analysis by considering 44 BBH candidates including GW190521 from GWTC-2 catalog (Abbott et al. 2021a). They also found that GW190521 is favored to be a 1g+2g merger over a 1g+1g merger with an odds ratio spanning 200 to 340, and a 2g+2g merger over a 1g+1g merger with an odds ratio spanning 700 to 1200 (assuming a cluster with $V_{\text{esc}} \approx 300$ km/s).

Considering that the LIGO, Virgo, and KAGRA (LVK) detectors are expected to detect hundreds of BBHs (Abbott et al. 2018), some of these mergers might be hierarchical in origin. It is therefore pertinent to ask the following question: *Given an observed BBH merger, can we unravel its merger history, assuming it was formed hierarchically?* This question involves two distinct issues. The first is the development of a method to go back, generation by generation, through the merger history of an observed BBH. This process starts by using the parameters of the components of an observed BBH to estimate the parameters of its potential “parents” (the binaries constituting the prior “generation” who merged to produce the observed components). In principle, this could be repeated to infer the parameters of the next prior merger generation (i.e., the “grandparents” of the observed binary). This is accomplished via the reasonable assumption that the relativistic merger dynamics is accurately described by Einstein’s general relativity. Numerical relativity (NR) simulations of BBHs can accurately predict the mass, spin, and kick velocity of the merger remnant BH as a function of the component BH masses and spins (Pretorius 2005; Campanelli et al. 2006; Baker et al. 2006; Lousto et al. 2010). These predictions, combined with measurements (via LVK observations) of the component masses and spins, allow us to track the properties of the parent BBHs of each component of an observed binary. However, measurement uncertainties on the system parameters—especially the

spins—restrict our ability to precisely track the merger history.

The second issue related to the posed question is how to deduce the *absolute* generation of each BH in a merger tree. For example, while one can develop a procedure to “step backwards” generation-by-generation through a merger tree, in many cases this process cannot be iterated back to the original first-generation (1g) black holes that formed from stellar collapse. Hence, one cannot easily determine if a given BBH in the merger tree represents (for example) a first (1g), second (2g), or third (3g) generation binary. Addressing this issue will require astrophysical insights about stellar collapse and the dynamics of BHs in clusters, which is beyond this work’s scope. Here, we will focus on the first issue—whereby given the parameters (and associated uncertainties) of a BH in a binary of generation N , we determine the component parameters of the prior $(N - 1)$ generation binary.

The issue of determining the parent binary properties of the member of a detected binary BH was partly addressed in Baibhav et al. (2021) by making use of BH spin measurements. The authors studied the constraints on the possible parents of the primary component of GW190412 (Abbott et al. 2020c) using NR fits (Barausse & Rezzolla 2009) for the remnant spins only. Similarly, Barrera & Bartos (2022) inferred the masses of the parents and grandparents of GW190521 using NR fits (Healy et al. 2014) for the remnant masses only (ignoring the spins, which are poorly determined). Barrera & Bartos (2024) showed that the neglect of spins is justified by using the NR fits in Tichy & Marronetti (2007). While this work was being finalized, an independent study by Araújo-Álvarez et al. (2024) also estimated the masses, spins, and recoil velocity of the parents of GW190521 using mass and spin posteriors and NR fits developed in Varma et al. (2019b,a) and using a Bayesian inference framework.

Here we provide a self-consistent Bayesian framework for inferring the properties of the ancestors of any BH using *both* the masses and spins of the binary constituents (assuming it is formed via a hierarchical merger). A key ingredient of this method is the state-of-the-art NR fits from Barausse et al. (2012); Hofmann et al. (2016); Varma et al. (2019b,a), which relate the binary component parameters to the mass, spin, and kick of the remnant. Our proposed Bayesian framework back-propagates the posterior distributions on the mass and spin of the candidate BH and identifies possible ‘parent’ binary configurations that are consistent with them. To assess the accuracy of our proposed method, we perform a series of injection studies whereby

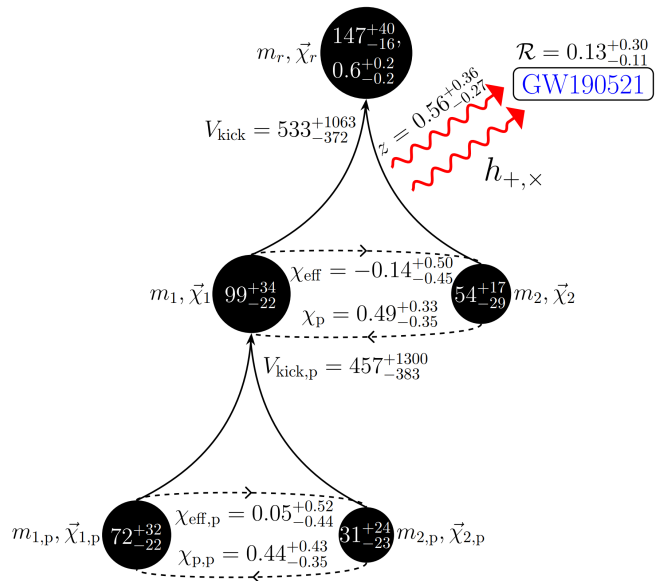


Figure 1. A schematic depiction of the possible merger history of GW190521 as inferred by our method. The middle of the figure depicts the binary components of GW190521, indicating the masses (in units of solar masses, M_{\odot}) as well as the effective dimensionless spin parameters (χ_{eff} , χ_p) as inferred from the LVK Collaboration analysis. The lower part of the figure shows the analogous parameters ($m_{1,p}$, $m_{2,p}$, $\chi_{\text{eff},p}$, $\chi_{p,p}$) for the parents of the primary component of GW190521. Those values are inferred via the method described in Section 2 and are among the main results of this paper. The numbers shown here quote the median parameter values, as well as the upper and lower limits of the 90% credibility interval of the inferred posteriors. We also show the redshift and merger rate (in units of $\text{Gpc}^{-3}\text{yr}^{-1}$) for GW190521, as well as the kick magnitude for the primary (in km/s).

multiple hierarchical merger trees are constructed, with noise artificially added to the parameters of the final binary in the tree. The tree is then reconstructed via our Bayesian framework, producing posterior probability distributions for the parameters of the “parent” and “grandparent” members of the tree. We then apply our method to GW190521, GW200220_061928 (hereafter GW200220), and GW190426_190642 (hereafter GW190426), three high-mass BBH mergers in GWTC-3 (the third gravitational-wave transient catalog) (Abbott et al. 2023b).

To illustrate our results, we show the possible merger history of GW190521 in Figure 1. Our method infers the masses and spins of the components of the parent binary that produced the primary component of GW190521. We also estimate the kick imparted to GW190521’s primary at the time of its formation. Our results are consistent with Baibhav et al. (2021); Barrera & Bartos (2022, 2024). However, because we make use of both the mass

and spin posteriors, our results provide comparatively tighter constraints. Our results are also in agreement with the findings of [Araújo-Álvarez et al. \(2024\)](#) when they consider quasi-circular scenario for GW190521.

The rest of the paper is organized as follows: In Section 2, we present our Bayesian inference framework for estimating the parameters of the parent BBH of a hierarchical candidate BH. We explain our choice of priors on various parameters in Section 3. Section 4 presents results from a simulated injection campaign. Results from the analysis of the three observed hierarchical candidate BHs mentioned above is reported in Section 5. Finally, in Section 6 we present conclusions and directions for future work.

2. GENEALOGICAL CONSTRUCTION METHOD

If one or both of the companion black holes in a binary black hole merger might have formed hierarchically, then we want to figure out the characteristics of the parent binary systems that resulted in the creation of those black holes. Suppose m_{obs} is the source-frame mass and χ_{obs} is the dimensionless spin parameter of a particular hierarchically-formed BH candidate (or, hierarchical candidate ‘hc’ for short) inferred from gravitational-wave (GW) data d . We denote those parameters via

$$\vec{\theta}_{\text{hc}} \equiv \{m_{\text{obs}}, \chi_{\text{obs}}\}. \quad (1)$$

We also denote $\vec{\theta}_{\text{p}}$ as the set of all parameters needed to describe the parent BBH of the hierarchical BH candidate with parameters $\vec{\theta}_{\text{hc}}$:

$$\vec{\theta}_{\text{p}} \equiv \{m_{1,\text{p}}, \vec{\chi}_{1,\text{p}}, m_{2,\text{p}}, \vec{\chi}_{2,\text{p}}\}, \quad (2)$$

where $m_{1,\text{p}}$, $\vec{\chi}_{1,\text{p}}$, $m_{2,\text{p}}$, and $\vec{\chi}_{2,\text{p}}$ are the masses and dimensionless spin angular momentum vectors of the primary² and secondary of the parent BBH, respectively. Note that the subscript ‘p’ always denotes ‘parent’ (not primary). We assume that the binary is circular,³ and the parameters are defined at a reference time $t = -100M_{\text{p}}$, where $t = 0$ denotes the merger and $M_{\text{p}} = m_{1,\text{p}} + m_{2,\text{p}}$.

We are interested in estimating the posterior probability distribution function $p(\vec{\theta}_{\text{p}}|d)$ of the masses and spin

² Throughout, we denote the more massive BH in a binary as the primary and labelled with a “1”.

³ This is a reasonable assumption since there are no high-confidence detections of eccentricity in the binaries reported in GWTC-3 (see, however, [Romero-Shaw et al. \(2020\)](#); [Gayathri et al. \(2022\)](#); [Romero-Shaw et al. \(2021\)](#); [O’Shea & Kumar \(2021\)](#); [Gupte et al. \(2024\)](#)). Once accurate NR fits accounting for eccentricity are available, this method can easily use them instead of quasi-circular NR fits.

parameters of the parent BBH given the GW data d for the observed BBH. From Bayes’ theorem, we have

$$p(\vec{\theta}_{\text{p}}|d) = \frac{\mathcal{L}(d|\vec{\theta}_{\text{p}}) \pi(\vec{\theta}_{\text{p}})}{\mathcal{Z}}, \quad (3)$$

where $\mathcal{L}(d|\vec{\theta}_{\text{p}})$ is the likelihood function of the data d given the parameters of the parent BBH $\vec{\theta}_{\text{p}}$, $\pi(\vec{\theta}_{\text{p}})$ is the prior probability density function for $\vec{\theta}_{\text{p}}$, and $\mathcal{Z} \equiv \int \mathcal{L}(d|\vec{\theta}_{\text{p}}) \pi(\vec{\theta}_{\text{p}}) d\vec{\theta}_{\text{p}}$ is the marginal likelihood or evidence. The likelihood function can be expressed as

$$\mathcal{L}(d|\vec{\theta}_{\text{p}}) = \int \mathcal{L}(d|\vec{\theta}_{\text{hc}}) p(\vec{\theta}_{\text{hc}}|\vec{\theta}_{\text{p}}) d\vec{\theta}_{\text{hc}}, \quad (4)$$

where, $p(\vec{\theta}_{\text{hc}}|\vec{\theta}_{\text{p}})$ is the probability distribution function of $\vec{\theta}_{\text{hc}}$ given the value of $\vec{\theta}_{\text{p}}$. Also by Bayes’ theorem, we have

$$p(\vec{\theta}_{\text{hc}}|d) = \frac{\mathcal{L}(d|\vec{\theta}_{\text{hc}}) \pi(\vec{\theta}_{\text{hc}})}{\mathcal{Z}_{\text{hc}}(d)}, \quad (5)$$

where $p(\vec{\theta}_{\text{hc}}|d)$ and $\pi(\vec{\theta}_{\text{hc}})$ are the posterior and the prior distributions of $\vec{\theta}_{\text{hc}}$, $\mathcal{L}(d|\vec{\theta}_{\text{hc}})$ is the likelihood of the data d given that the GW signal contains a BH with parameters $\vec{\theta}_{\text{hc}}$, and $\mathcal{Z}_{\text{hc}}(d) \equiv \int \mathcal{L}(d|\vec{\theta}_{\text{hc}}) \pi(\vec{\theta}_{\text{hc}}) d\vec{\theta}_{\text{hc}}$ is the evidence for the data d containing a BH with parameters $\vec{\theta}_{\text{hc}}$. We can now recast Equation (4) as

$$\mathcal{L}(d|\vec{\theta}_{\text{p}}) = \int \frac{p(\vec{\theta}_{\text{hc}}|d) \mathcal{Z}_{\text{hc}}(d)}{\pi(\vec{\theta}_{\text{hc}})} p(\vec{\theta}_{\text{hc}}|\vec{\theta}_{\text{p}}) d\vec{\theta}_{\text{hc}}. \quad (6)$$

Given the mass and spin parameters of the parent BBH, the mass and the spin of the remnant BH (i.e., the hierarchically formed candidate BH with parameters $\vec{\theta}_{\text{hc}}$) can be uniquely predicted with NR fitting formulas for the remnant mass and spin ([Barausse et al. 2012](#); [Hofmann et al. 2016](#); [Varma et al. 2019b,a](#)), modulo the uncertainties on the NR fits.⁴ Therefore, the probability density function $p(\vec{\theta}_{\text{hc}}|\vec{\theta}_{\text{p}})$ can be taken to be a delta function,

$$p(\vec{\theta}_{\text{hc}}|\vec{\theta}_{\text{p}}) = \delta(\vec{\theta}_{\text{hc}} - \vec{F}(\vec{\theta}_{\text{p}})), \quad (7)$$

where $\vec{F}(\vec{\theta}_{\text{p}}) \equiv \{m_{\text{f}}^{\text{NR}}(\vec{\theta}_{\text{p}}), \chi_{\text{f}}^{\text{NR}}(\vec{\theta}_{\text{p}})\}$ denotes the NR fits that map the parent parameters $\vec{\theta}_{\text{p}}$ to the final mass and spin of the remnant. Rewriting the above equation as

$$p(\vec{\theta}_{\text{hc}}|\vec{\theta}_{\text{p}}) = \delta(m_{\text{obs}} - m_{\text{f}}^{\text{NR}}(\vec{\theta}_{\text{p}})) \delta(\chi_{\text{obs}} - \chi_{\text{f}}^{\text{NR}}(\vec{\theta}_{\text{p}})), \quad (8)$$

⁴ The errors (due to the numerical fitting) in the NR final mass/spin relations are smaller than typical statistical errors in the mass and spin measurements made with current GW detectors.

plugging into Equation (6), and evaluating the integral over $\vec{\theta}_{\text{hc}} \equiv \{m_{\text{obs}}, \chi_{\text{obs}}\}$ yields

$$\mathcal{L}(d|\vec{\theta}_p) = \mathcal{Z}_{\text{hc}}(d) \frac{p(\vec{\theta}_{\text{hc}}|d)}{\pi(\vec{\theta}_{\text{hc}})} \Big|_{\vec{\theta}_{\text{hc}}=\vec{F}(\vec{\theta}_p)}. \quad (9)$$

Substituting Equation (9) into Equation (3) then provides an expression for $p(\vec{\theta}_p|d)$:

$$p(\vec{\theta}_p|d) = \pi(\vec{\theta}_p) \frac{\mathcal{Z}_{\text{hc}}(d)}{\mathcal{Z}} \frac{p(\vec{\theta}_{\text{hc}}|d)}{\pi(\vec{\theta}_{\text{hc}})} \Big|_{\vec{\theta}_{\text{hc}}=\vec{F}(\vec{\theta}_p)}. \quad (10)$$

Moreover, note that the evidence $\mathcal{Z}(d)$ also contains $\mathcal{Z}_{\text{hc}}(d)$, which cancels out with $\mathcal{Z}_{\text{hc}}(d)$ in the numerator. [This follows from Equation (9) and the above definition of \mathcal{Z} , yielding $\mathcal{Z}(d) = \mathcal{Z}_{\text{hc}}(d) \int \pi(\vec{\theta}_p) \frac{p(\vec{\theta}_{\text{hc}}|d)}{\pi(\vec{\theta}_{\text{hc}})} \Big|_{\vec{\theta}_{\text{hc}}=\vec{F}(\vec{\theta}_p)} d\vec{\theta}_p$.] Hence, Equation (10) further simplifies to

$$p(\vec{\theta}_p|d) = \frac{\pi(\vec{\theta}_p)}{\mathcal{Z}_p(d)} \frac{p(\vec{\theta}_{\text{hc}}|d)}{\pi(\vec{\theta}_{\text{hc}})} \Big|_{\vec{\theta}_{\text{hc}}=\vec{F}(\vec{\theta}_p)}, \quad (11)$$

where, $\mathcal{Z}_p(d) \equiv \int \pi(\vec{\theta}_p) \frac{p(\vec{\theta}_{\text{hc}}|d)}{\pi(\vec{\theta}_{\text{hc}})} \Big|_{\vec{\theta}_{\text{hc}}=\vec{F}(\vec{\theta}_p)} d\vec{\theta}_p$ is the rescaled evidence.

Equation (11) acts as the master equation for our method. The posteriors $p(\vec{\theta}_p|d)$ for the masses and spins of the parent BHs can be deduced from $p(\vec{\theta}_{\text{hc}}|d)$ (which is known from inference on the GW data from the observed BBH) and NR fits for the final mass/spin relations $\vec{F} = \{m_f^{\text{NR}}, \chi_f^{\text{NR}}\}$. Since the posteriors and priors on $\vec{\theta}_{\text{hc}}$ are provided as discrete samples, we use a probability density estimator fit to these samples for constructing $p(\vec{\theta}_{\text{hc}}|d)$ and $\pi(\vec{\theta}_{\text{hc}})$. To generate discrete samples for the probability distribution function $p(\vec{\theta}_p|d)$, we used the Bayesian parameter inference library `bilby` (Ash-ton et al. 2019) with the `dynesty` (Speagle 2020) sampler (which uses the nested sampling algorithm (Skilling 2004)). Our choice of priors $\pi(\vec{\theta}_p)$ is explained in the next section.

For inverse mass ratios (here, the mass ratio of binary is defined as the ratio of secondary and primary mass) less than 6, we used the numerical fits for the BBH remnant mass and spin given in Varma et al. (2019a); for inverse mass ratios greater than 6 we use the fits in Barausse et al. (2012); Hofmann et al. (2016). The dimensionless spin vectors of the parent BBHs can be characterized in terms of 5 parameters: the dimensionless spin magnitudes, $\chi_{1,p}$ and $\chi_{2,p}$; the angles between the spin vectors and the orbital angular momentum $\theta_{1,p}$ and $\theta_{2,p}$; and the difference between the azimuthal angles of the two spin vectors, $\phi_{12,p}$. These angles are defined at a reference time $t = -100M_p$. (We assume $G = c = 1$

throughout the paper.) The complete set of parameters that describe any parent BBH is hence given by

$$\vec{\theta}_p = \{m_{1,p}, m_{2,p}, \chi_{1,p}, \chi_{2,p}, \cos \theta_{1,p}, \cos \theta_{2,p}, \phi_{12,p}\}. \quad (12)$$

By iterating the method described above once more, we can also estimate the properties of the ‘grandparent BBH’ (denoted by $\vec{\theta}_{\text{gp}}$), assuming that the parent BHs were also likely to have formed hierarchically. For instance, if the primary of the parent BBH is a hierarchical candidate (i.e., $\vec{\theta}_{\text{hc}} \equiv \{m_{1,p}, \chi_{1,p}\}$), then the posterior distribution on $\vec{\theta}_{\text{gp}}$, $p(\vec{\theta}_{\text{gp}}|d)$, will be obtained by substituting $\vec{\theta}_{\text{hc}} \rightarrow \{m_{1,p}, \chi_{1,p}\}$ and $\vec{\theta}_p \rightarrow \vec{\theta}_{\text{gp}}$ in Equation (11). In principle, this backward evolution can go on until we have reached a first-generation BH (or the posterior distribution of the properties of the ancestors becomes uninformative).

3. CHOICE OF PRIORS

Though we have derived a likelihood function for the problem, the choice of *astrophysically-motivated* priors is not straightforward. This is because astrophysically-motivated priors require us to know the *absolute* merger generation of the observed BH whose history we are trying to reconstruct (i.e., we need to know if the observed BH is a 2g, 3g, or higher generation BH). Determining this is complicated because:

1. The mass distributions of the earlier-generation stellar-mass BBHs in metal-poor star clusters are degenerate with the mass distributions of the higher-generation stellar-mass BBHs in metal-rich star clusters (Chattopadhyay et al. 2022), making it difficult to infer the merger generation (see Figure 2 of Chattopadhyay et al. 2023).
2. The spin distributions of higher-generation stellar-mass BBHs are very similar to each other, peaking at ~ 0.7 with a width that weakly depends on the merger-generation (Pretorius 2005; Gerosa & Berti 2017; Fishbach et al. 2017; Zevin & Holz 2022). This makes any unique inference about the merger generation a daunting task.

Any choice of priors along the above lines would lead to implicit assumptions about the properties of the cluster (such as metallicity) in which the merger took place. Therefore, it is more convenient for us to assume priors that are agnostic to the details of the host astrophysical environments. Our choice of prior on $\vec{\theta}_p$ is only based on our knowledge of BBH dynamics in general relativity and is described below.

We assume that the minimum and maximum possible mass ($m_{\text{obs}}^{\text{min}}, m_{\text{obs}}^{\text{max}}$) that the hierarchical candidate

Parameters	Prior ranges	Parameters	Prior ranges
$m_{1,p}$	$[\frac{M_p^{\min}}{2}, M_p^{\max} - m_{\text{BH}}^{\min}]$	$\chi_{2,p}$	$[0, 0.99]$
$m_{2,p}$	$[m_{\text{BH}}^{\min}, \frac{M_p^{\max}}{2}]$	$\cos \theta_{1,p}$	$[-1, 1]$
q_p	$[\frac{m_{\text{BH}}^{\min}}{M_p^{\max} - m_{\text{BH}}^{\min}}, 1.0]$	$\cos \theta_{2,p}$	$[-1, 1]$
$\chi_{1,p}$	$[0, 0.99]$	$\phi_{12,p}$	$[0, 2\pi]$

Table 1. The initial ranges for the priors on different mass and spin parameters of the parent BBHs.

BH can have is given by the lower and upper limits (respectively) of the 95% credibility interval of the posterior of m_{obs} .⁵ Similarly, the minimum and maximum possible spin magnitude ($\chi_{\text{obs}}^{\min}, \chi_{\text{obs}}^{\max}$) that the hierarchical candidate BH can have is given by the lower and the upper limits of the 95% credibility interval of the χ_{obs} posterior.⁶ The maximum possible value for the radiated energy from a binary system is $\sim 10\%$ of its total mass (Barausse et al. 2012). Therefore, the maximum possible total mass of the parent binary is $M_p^{\max} = \frac{1.0}{0.9} \times m_{\text{obs}}^{\max}$. The minimum possible total mass of the parent binary is $M_p^{\min} = m_{\text{obs}}^{\min}$ (assuming a negligible mass loss from the parent binary). The minimum possible mass of a BH is denoted by m_{BH}^{\min} and we choose it to be $5M_{\odot}$ in our study. The maximum possible value of $m_{1,p}$ is $M_p^{\max} - m_{\text{BH}}^{\min}$; this occurs when the total mass of the parent binary takes its maximum possible value (M_p^{\max}) and the secondary takes its minimum possible value (m_{BH}^{\min}). The minimum possible value of $m_{1,p}$ will be $\frac{M_p^{\min}}{2}$; this happens when the total mass of the parent binary takes its minimum possible value (M_p^{\min}) and the mass ratio of the parent binary is unity ($m_{1,p} = m_{2,p}$). Similarly, the maximum possible value of $m_{2,p}$ will be $\frac{M_p^{\max}}{2}$; this is when the total mass of the parent binary takes its maximum possible value (M_p^{\max}) and the mass ratio is again unity. Hence, the allowed ranges for the primary mass $m_{1,p}$, secondary mass $m_{2,p}$, and the mass ratio $q_p \equiv m_{2,p}/m_{1,p}$ of the parent BBH are given by $[M_p^{\min}/2, M_p^{\max} - m_{\text{BH}}^{\min}]$, $[m_{\text{BH}}^{\min}, M_p^{\max}/2]$, and $[m_{\text{BH}}^{\min}/(M_p^{\max} - m_{\text{BH}}^{\min}), 1.0]$, respectively. The ini-

⁵ The released LVK posterior samples of individual masses of the binary are derived assuming uniform priors on the detector-frame masses (which do not lead to uniform priors on the component masses of the binary). Therefore, to obtain the posterior samples of m_{obs} that assumes a uniform prior, we do the prior-reweighting of the LVK samples of $\{m_{\text{obs}}, \chi_{\text{obs}}\}$.

⁶ Note that, we use 95% credible intervals for obtaining the prior boundaries, while the standard practice in the GW community is to use 90% credible ranges.

tial ranges for the priors on different spin parameters (as well as the mass parameters) are given in Table 1.

We also note the following properties of BBHs (implicit in the NR fits) that further refine these prior boundaries, eliminating unphysical regions of the parameter space.

1. In the parameter space spanned by $\{m_{1,p}, m_{2,p}, \chi_{1,p}, \chi_{2,p}, \phi_{12,p}\}$, the remnant spin is maximal when both the spin vectors are aligned with respect to the orbital angular momentum, i.e., $\cos \theta_{1,p} = \cos \theta_{2,p} = 1$ (Baibhav et al. 2021). Therefore, the parameter space where $\chi_f^{\text{NR}}(m_{1,p}, m_{2,p}, \chi_{1,p}, \chi_{2,p}, \cos \theta_{1,p} = 1, \cos \theta_{2,p} = 1, \phi_{12,p}) < \chi_{\text{obs}}^{\min}$, is ruled out.
2. Using the NR fits of Barausse & Rezzolla (2009), Baibhav et al. (2021) found that in the parameter space $q_p \gtrsim 0.28(\chi_{1,p} + q_p^2 \chi_{2,p})$, the remnant spin is minimal when both the spin vectors are anti-aligned with respect to the orbital angular momentum; i.e., $\cos \theta_{1,p} = \cos \theta_{2,p} = -1$ [see Section IIIA and Equations (11) and (12) of Baibhav et al. (2021) for a detailed discussion.]. Whereas, in the parameter space $q_p \lesssim 0.28(\chi_{1,p} + q_p^2 \chi_{2,p})$, Baibhav et al. (2021) found that the remnant spin is minimal when the primary BH is anti-aligned and the secondary BH is aligned; i.e., $\cos \theta_{1,p} = -1, \cos \theta_{2,p} = 1$. Hence, for $q_p \gtrsim 0.28(\chi_{1,p} + q_p^2 \chi_{2,p})$, the region of parameter space with $\chi_f^{\text{NR}}(m_{1,p}, m_{2,p}, \chi_{1,p}, \chi_{2,p}, \cos \theta_{1,p} = -1, \cos \theta_{2,p} = -1, \phi_{12,p}) > \chi_{\text{obs}}^{\max}$ is ruled out. Similarly, for $q_p \lesssim 0.28(\chi_{1,p} + q_p^2 \chi_{2,p})$, the region of parameter space with $\chi_f^{\text{NR}}(m_{1,p}, m_{2,p}, \chi_{1,p}, \chi_{2,p}, \cos \theta_{1,p} = -1, \cos \theta_{2,p} = 1, \phi_{12,p}) > \chi_{\text{obs}}^{\max}$ is ruled out.
3. In the parameter space spanned by $\{m_{1,p}, m_{2,p}, \chi_{1,p}, \chi_{2,p}, \phi_{12,p}\}$, the remnant mass is maximal (i.e., the radiated energy is minimal) when both the spin vectors are anti-aligned with respect to the orbital angular momentum, i.e., $\cos \theta_{1,p} = \cos \theta_{2,p} = -1$ (Barausse et al. 2012). Therefore, the parameter space where $m_f^{\text{NR}}(m_{1,p}, m_{2,p}, \chi_{1,p}, \chi_{2,p}, \cos \theta_{1,p} = -1, \cos \theta_{2,p} = -1, \phi_{12,p}) < m_{\text{obs}}^{\min}$ is ruled out.
4. Similarly, the remnant mass is minimal (i.e., the radiated energy is maximal) when both the spin vectors are aligned with respect to the orbital angular momentum, i.e., $\cos \theta_{1,p} = \cos \theta_{2,p} = 1$ (Barausse et al. 2012). Hence, the parameter space where $m_f^{\text{NR}}(m_{1,p}, m_{2,p}, \chi_{1,p}, \chi_{2,p}, \cos \theta_{1,p} = 1, \cos \theta_{2,p} = 1, \phi_{12,p}) > m_{\text{obs}}^{\max}$ is ruled out.

To determine the priors on $\vec{\theta}_p$ [i.e., $\pi(\vec{\theta}_p)$ in Equation (3)], we uniformly sample from the allowed parameter space of $\vec{\theta}_p$ while imposing the above conditions. Combined with Equation (3), this allows us to obtain the posteriors of the properties of the parent BBH.

4. INJECTION STUDY

Having outlined the details of our method, we next validate it using simulated “injections.” The objective is to confirm that we can reliably reconstruct the elements of a merger chain (and if so, with what precision). First, to explore different regions of the parameter space, we consider different combinations of the component masses ($m_{1,p}$, $m_{2,p}$) and spin magnitudes ($\chi_{1,p}$, $\chi_{2,p}$) for parent BBHs tabulated in Table 2 of Appendix A. Tables and Figures for this section are displayed in Appendix A to improve readability. The spin angles are drawn randomly from an isotropic distribution; the corresponding effective spin and spin precession parameters are also listed in Table 2 of Appendix A⁷. For each case, we calculate the final mass ($m_{f,p}$) and final spin ($\chi_{f,p}$) using the NR fits mentioned in Section 2. To assess the effectiveness of our method, we use these values and generate mock posterior samples of m_{obs} from a Gaussian distribution with mean $m_{f,p}$ and standard deviation $0.05 \times m_{f,p}$. Similarly, we generate mock posterior samples of χ_{obs} from a Gaussian distribution with mean $\chi_{f,p}$ and standard deviation $0.1 \times \chi_{f,p}$.⁸ Next, to apply our method to this noisy synthetic data, we feed these samples of m_{obs} and χ_{obs} into Equation (11) to infer the parameters of the parent BBH $p(\vec{\theta}_p|d)$ in each case. The results from this injection analysis are tabulated in Table 2 of Appendix A, which shows the 90% credible intervals on the recovered posteriors of the masses, spin parameters, and kick speeds of the simulated parent binaries. The injected values of different parameters of the parent BBHs considered here are recovered well within 90% credibility.

Next, we repeat this procedure except we only generate mock posterior samples for m_{obs} (using the same approach); we assume that the spin posteriors are entirely uninformative and do not generate posteriors for χ_{obs} . We again proceed to estimate $p(\vec{\theta}_p|d)$ via Equation (11).

⁷ Given the limited information in the individual spin posteriors, it is more instructive to report posteriors for the effective spin variables $\chi_{\text{eff}} \equiv (\chi_1 \cos \theta_1 + q \chi_2 \cos \theta_2)/(1 + q)$ (Damour 2001; Racine 2008) and $\chi_p \equiv \max(\chi_1 \sin \theta_1, q \frac{3+4q}{4+3q} \chi_2 \sin \theta_2)$ (Schmidt et al. 2015), as is done in the standard compact binary inference problem.

⁸ These error ranges are comparable to the corresponding measurement errors for GW190412 (Abbott et al. 2020c) and GW190814 (Abbott et al. 2020d).

The results of this injection analysis are tabulated in Table 3 of Appendix A, which is analogous to Table 2 of Appendix A. As expected, the constraints on the different parameters of the parent binaries from this analysis (which uses only mass estimates of the remnant BHs) are weaker than the previous analysis (which uses both mass and spin estimates of the remnant BHs). Although the injected values of the parameters of the parent binaries are recovered within 90% credibility, the median values of the posteriors are slightly offset from the injected values for some cases (especially for unequal-mass and highly spinning parent binaries). Therefore, one has to be very careful when computing the properties of parent binaries based on the estimates of their remnant masses only, as this can lead to potential biases.

We then use the SPHM model from Mahapatra et al. (2022) to generate mock 1g+3g merger chains in different clusters.⁹ The SPHM model takes the initial mass function (IMF) and spin distributions of first-generation (1g) BHs, assumes a pairing probability function, and applies NR fitting formulas for the mass, spin, and kick speed of the merger remnant to predict the mass and spin distributions of higher generation BBHs formed in a cluster with escape speed V_{esc} (Mahapatra et al. 2022). We first calculate the IMF of BHs inside a cluster with metallicity $Z = 0.00015$ and escape speed $V_{\text{esc}} = 400$ km/s. To calculate this IMF, we sampled the masses of the BH stellar progenitors from the Kroupa initial mass function, $p(m_*) \propto m_*^{-2.3}$ (Kroupa 2001; Salpeter 1955), with m_* corresponding to initial stellar masses in the range $20M_{\odot}$ – $130M_{\odot}$. Then, the individual stars are evolved to BHs using the Single Stellar Evolution package (Hurley et al. 2000); this includes updated prescriptions for stellar winds and mass loss (Vink et al. 2001) and the pair-instability process in massive stars (Spera & Mapelli 2017). Here, we consider a uniform distribution between $[0, 0.99]$ for the dimensionless spin magnitude χ of a 1g BHs. We provide these IMF and spin distributions for 1g BHs, along with the pairing probability function $p^{\text{pair}}(m_2|m_1) \propto M_{\text{tot}}^6$ ($M_{\text{tot}} = m_1 + m_2$ is the total mass of the binary), to the SPHM to generate mock 1g+3g merger chains. We generate ten mock 1g+3g merger chains. In each chain, we take the masses (m_1^{3g}) and spin magnitudes (χ_1^{3g}) of the 3g BHs (i.e., the remnants from 1g+2g mergers), and generate mock posterior samples for m_{obs} from a Gaussian distribution with mean m_1^{3g} and standard deviation $0.05 \times m_1^{3g}$. Sim-

⁹ Here the notation 1g+3g refers to a binary composed of a first generation (1g) BH (i.e., one formed from stellar collapse) and third generation (3g) BH (i.e., one formed from two prior BBH mergers).

ilarly, we generate mock posterior samples for the spin magnitudes χ_{obs} assuming a Gaussian distribution with mean χ_1^{3g} and standard deviation $0.05 \times \chi_1^{3g}$. Next, we feed these mock posterior samples [i.e., $p(\vec{\theta}_{\text{hc}}|d)$] into Equation (11) to estimate the posteriors $p(\vec{\theta}_{\text{p}}|d)$ on the parameters $\vec{\theta}_{\text{p}}$ of the parent binaries (i.e., 1g+2g mergers). Further, we feed the obtained posterior samples for the masses and the spins of the parent BHs (i.e., 2g BHs) into Equation (11) to derive the posteriors $p(\vec{\theta}_{\text{gp}}|d)$ for the parameters $\vec{\theta}_{\text{gp}}$ of the grandparent binaries (i.e., 1g+1g mergers).

Table 4 of Appendix A shows the results from this injection analysis of mock 1g+3g merger chains in a cluster with metallicity $Z = 0.00015$ and escape speed $V_{\text{esc}} = 400$ km/s. There we find the 90% credible intervals on the recovered posteriors of the masses, spin parameters, and kick speeds for the simulated parent and grandparent binaries. We show the reconstruction of the parameters of parent and grandparent binaries for one such 1g+3g merger chain in Figure 6 of Appendix A. We see that the injected values of different parameters of the parent and grandparent binaries are recovered within 90% credibility. However, in some cases, the median values of the recovered posteriors for the masses of the grandparent binaries are offset from their injected values. Moreover, the fractional error bars on different parameters of the grandparent binaries are worse compared to the parent binaries. Therefore, we can not estimate the properties of previous merger generations backwards to an arbitrary number of generations.

We perform a similar injection study with mock 1g+3g merger chains for a cluster with metallicity $Z = 0.0225$ and escape speed $V_{\text{esc}} = 400$ km/s. Those results are tabulated in Table 5 of Appendix A. The reconstruction of the parameters of the parent and grandparent binaries for one such 1g+3g merger chain are shown in Figure 7 of Appendix A. We see that in all of the cases considered here, the injected values of different parameters of the parent and grandparent binaries are recovered well within 90% credibility.

Our mock posteriors peak at the true values of the mass and spin parameters, which represent the ensemble average of the posterior over a large number of realizations. In reality, however, the presence of background noise causes the posteriors of each event, observed in a small number of detectors, to be shifted by a value drawn from the average posterior. Consequently, the inferred parameters of the parents for any one event will most likely not be centered around the true value but offset by the value drawn from the average posterior. The average properties of the parent black holes derived

for a large population of systems should be free from systematic biases seen in individual events.

These three different types of injection studies validate our method. We next apply our approach to the analysis of BBHs detected during the first three observing runs of LIGO/Virgo as reported in GWTC-3 (Abbott et al. 2021b).

5. ANALYSIS OF SELECTED GWTC-3 EVENTS

We now turn our attention to the analysis of selected GWTC-3 events. We choose events based on the criterion that at least one of the observed binary components should lie in the high mass gap (assumed here to be $\geq 60M_{\odot}$). To be more precise, mass posteriors of at least one of the component BHs should exclude a lower limit of $60M_{\odot}$ at 90% credibility. In this section, we also restrict our backward evolution for BBH parents to stop when the masses of both the components go below this $60M_{\odot}$ limit (again at 90% credibility). As hierarchical mergers can also produce BHs with masses smaller than the PISN/PPISN mass gap (in metal-rich clusters), this condition is primarily for algorithmic convenience and to restrict the considered GWTC-3 binaries to those most likely to contain a BH formed via hierarchical merger. The GWTC-3 catalog has three events that qualify for this analysis: GW190521¹⁰ (Abbott et al. 2020a), GW200220 (Abbott et al. 2023b) and GW190426 (Abbott et al. 2024). The first two events are part of the GWTC-3 catalog, while the third event GW190426¹¹ is a low-significance trigger listed in the deep and extended catalog of the LVK Collaboration (GWTC-2.1) (Abbott et al. 2024).

The properties of the ancestors of GW190521 from our analysis are presented in Figure 1; those for GW200220 and GW190426 are shown in Figure 2. The left and right panel of Figure 3 shows the inferred masses and effective spin parameters of the primary’s parent BHs, respectively. For all the three events, though the median mass of the parent BHs of the primary still lie above the PISN/PPISN mass gap, the lower limit has non-negligible support for $\leq 60M_{\odot}$; hence, based on the above-mentioned criteria, we do not evolve this system further back. Figure 4 shows the inferred retention probability of the primary BHs of the three events using

¹⁰ See Nitz & Capano (2021); Fishbach & Holz (2020); Chandra et al. (2024) which argue that unconventional choices of priors can alter the mass estimates of GW190521.

¹¹ There was also a neutron star-black hole candidate GW190426_152155 (Abbott et al. 2021a) that happened on the same day as the BBH candidate GW190426. That event is not considered here.

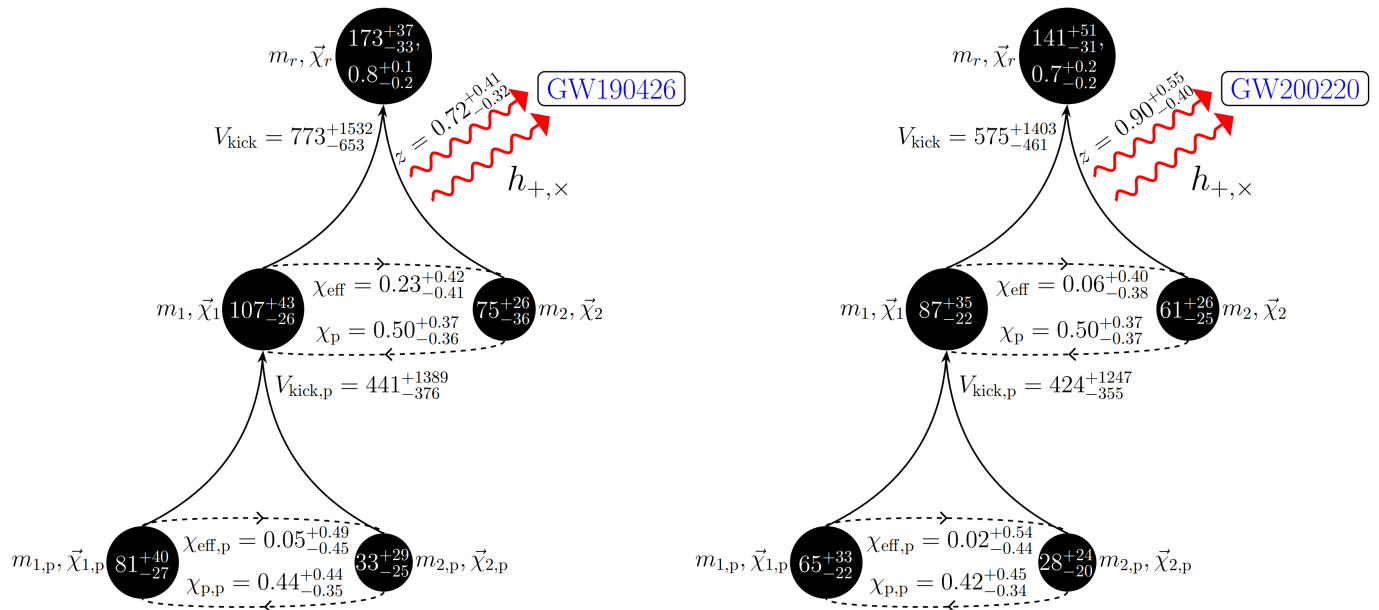


Figure 2. Depiction of the possible merger history of the primary components of GW190426 and GW200220 as inferred by our method. The notation and units are the same as in Figure 1.

estimates of the GW-induced kicks and assuming the parent binary resides in a dense environment.

There are three important messages from these plots:

1. The first step of the backward evolution of the three binaries results in parent BBHs whose primary components are of relatively high mass ($\gtrsim 40M_{\odot}$).
2. Parents of the primaries of all three events share similar properties, such as mass ratio, spin parameters, and kick speed.
3. Gravitationally bound environments with $V_{\text{esc}} \geq 100$ km/s are preferred sites to host these events.

Our method cannot tell whether these parent BHs themselves were products of previous mergers. As none of the parent BHs meet our criterion for further iteration, we do not ask whether they had a history of previous mergers. However, it may be possible to interpret these results in conjunction with stellar evolution and N -body simulations to gain further insights about the absolute generation of the parent black holes. For instance, if the parents are indeed first-generation BHs, they should have formed in environments that produce high-mass first-generation BHs in abundance (e.g., low metallicity clusters). Our current understanding of star clusters and their properties may help us better understand the history of these parent BHs. We do not undertake a study along these lines here.

The left panel of Figure 3 shows the two-dimensional inferred posterior probability distributions for the

masses of the parents of the primaries of the three considered BBH systems. The right panel shows the two-dimensional inferred posterior probability distributions for χ_{eff} and χ_p for the parent binaries. The contours indicate 90% and 50% credibility regions. The posteriors of the effective spin parameters in all three cases are seen to share similar features. This similarity may suggest that the parents of the primaries of the three events are of the same generation and/or originated from similar astrophysical environments.

Figure 4 shows the cumulative probability distribution function (CDF) for the kick speed of the primary of the three events¹². This can be straightforwardly mapped to the retention probability of the primary in a cluster with an escape speed V_{esc} as shown in Mahapatra et al. (2021). The typical ranges of the escape speeds of GCs and NSCs are shown as shaded regions. As can be read-off from Figures 1 and 2, the mass ratio and effective spin parameters of the parents of these three events are very similar to each other. Therefore, they have similar kick CDFs (and hence the same retention probabilities in a cluster). It is evident from Figure 4 that even GCs with very high escape speeds [$\sim \mathcal{O}(100$ km/s)] would not have retained the primaries as the retention probability

¹² To assess the information content in the inferred kick posteriors for the parent BBHs relative to the priors, we calculated the Jensen–Shannon (JS) divergence (Lin 1991). The JS divergences for kick posteriors of the parents of GW190521, GW190426, and GW200220 are 0.059, 0.060, and 0.055, respectively. These JS divergence values are above the threshold of 0.007 (used in Abbott et al. (2021a)) where posteriors are considered to be informative.

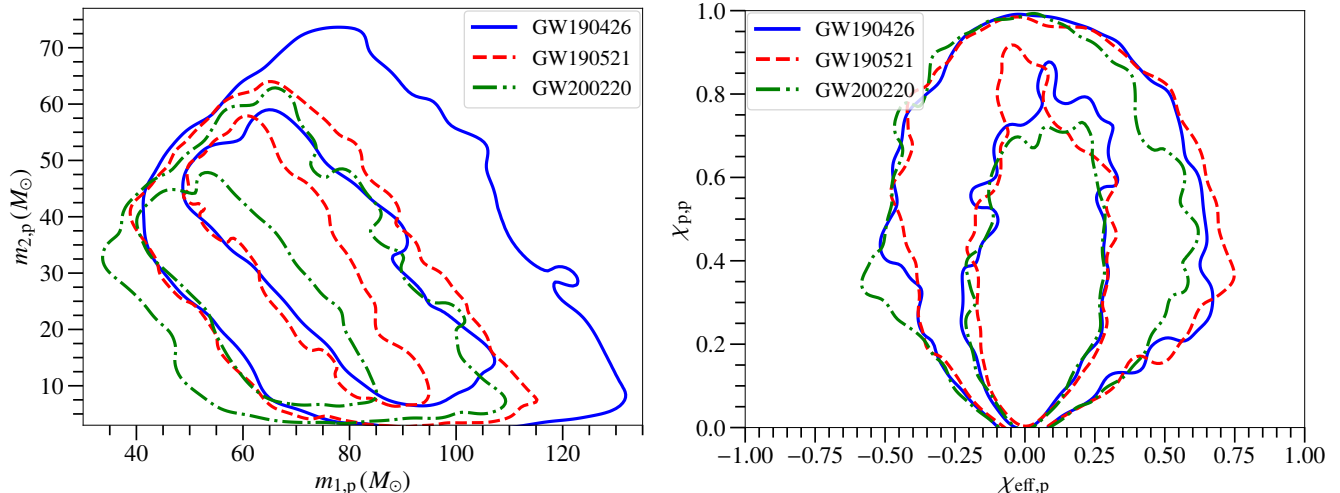


Figure 3. The left panel shows the inferred mass parameters (at 90% and 50% credibility) for the parent BBH whose merger produced the primary BHs of GW190521, GW200220, and GW190426. The right panel shows the corresponding inferred effective spin parameters (again at 90% and 50% credibility) for those parent binaries.

for clusters with such escape speeds is $\mathcal{O}(10\%)$ or less. This suggests that the three considered BBHs were unlikely to have merged in Milky Way-type GCs ($V_{\text{esc}} \sim 30$ km/s). The host environments for these mergers were more likely to be massive GCs, NSCs, or AGN discs.

If the selected GW events are produced from higher-generation mergers, it is natural to expect that a much larger number of lower generation mergers would occur in these clusters, since only a small fraction of these lower generation mergers would pair up to form a next-generation binary. It is then pertinent to ask if the LVK

events detected to date contain binaries that resemble the inferred parents of the three cases we consider here. Figure 5 compares the inferred masses of the parent BHs of the three considered systems with the masses of a few selected events from GWTC-3. Despite the errors associated with the parent BBH parameters, it is evident that there are indeed events in GWTC-3 that are at least consistent with the existence of a subpopulation of BBHs with inferred masses similar to those of the parent BBHs. A dedicated study that looks into the intrinsic rates of BBH mergers in different mass bins is needed to draw firmer conclusions beyond the broad consistency seen in this figure. Moreover, such a study should also include a detailed analysis of the binary spin parameters across the detected population and their correlation with mass. This will require a larger number of BBH detections from current and future LVK observing runs, and contributes to the science case for next-generation detectors like Cosmic Explorer (Reitze et al. 2019) and the Einstein Telescope (Sathyaprakash et al. 2012; Abbott et al. 2017).

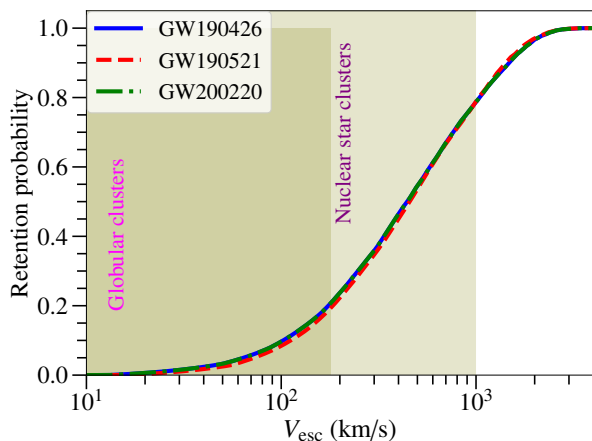


Figure 4. The retention probability of the primary BHs of GW190521, GW200220, and GW190426 as a function of a star cluster’s escape speed. The shaded regions on the right panel show the range of escape speeds for globular clusters and nuclear star clusters (Antonini & Rasio 2016). The retention probability is computed directly from the cumulative distribution function of the kick magnitude following Mahapatra et al. (2021).

6. CONCLUSIONS AND DISCUSSIONS

We have outlined a Bayesian inference framework that determines the genealogy of observed LIGO/Virgo BBHs, assuming the binary components were themselves formed via a binary BH merger. Our approach uses the measured masses and spins of the binary components to infer the masses and spins of their parent BBHs. The method makes use of the mapping—based on NR simulations—between initial and final configurations of a BBH merger. We validated our method by applying it to a mock data set that closely follows N -

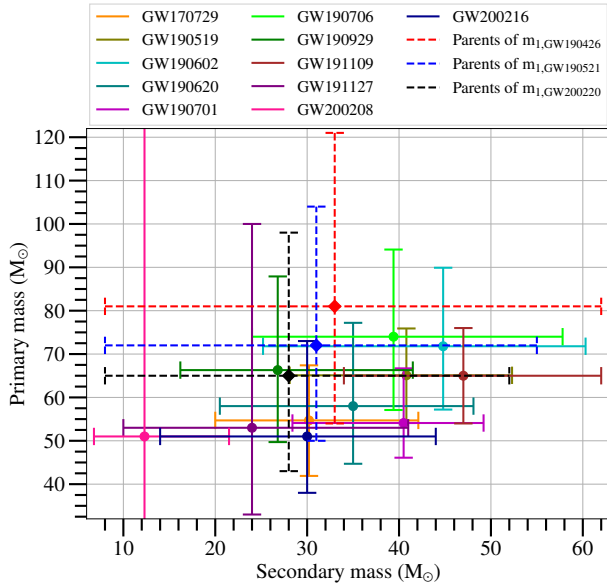


Figure 5. Masses of the parent BHs of the primaries of three considered BBH events, along with selected high-mass GW events from the GWTC-3 catalog. Error bars represent 90% credibility regions on the component masses.

body results for hierarchical mergers. We then applied this method to the primary components of GW190521, GW200220 and GW190426. These three LIGO/Virgo events were chosen because the 90% lower limit of their primary masses exclude $60M_{\odot}$, a typical value assumed for the lower end of the PISN/PPISN mass gap. Our main results for the potential merger history of these events are shown in Figures 1, 2, and 3.

We also find that the primary’s parent BBHs for the three GW events share very similar spin-effective parameters and kick magnitudes, potentially hinting that the three events are mergers of the same generation and occurred in similar astrophysical environments. We also showed that GWTC-3 contains BBHs whose masses coincide (within the measurement uncertainties) with those of the inferred parent BBHs for the three events studied here.

Note that our method reconstructs a merger history *assuming* the observed BBH was formed via a hierarchical merger. We do not attempt to statistically quantify whether the components of a detected BBH are hierarchically formed; rather, we provide an ancestral pathway assuming they had a merger history. By comparing the merger history with one predicted from N-body simulations, it may be possible to assign a probability of a given BBH having formed from a hierarchical merger (and to perhaps identify the most probable merger generation). This will be explored in detail in future work.

Inferring the redshift where the parent binary merged (and hence determining how long ago the merger took place) is an interesting follow-up. However, predicting the redshift of the parent binary requires us to adopt ingredients from the astrophysical modelling of dense star clusters. Specifically, we need to know the time scales associated with different physical processes in the host clusters. This will also be explored in future work.

ACKNOWLEDGMENTS

P.M. thanks Duncan MacLeod for his suggestions on various computing issues. P.M. thanks Juan Calderón Bustillo, Amanda Farah, Matthew Mould, and Koustav Chandra for insightful comments on the manuscript. We thank Zoheyr Doctor for critical reading of the manuscript and providing useful comments. P.M. and K.G.A. acknowledge the support of the Core Research Grant CRG/2021/004565 of the Science and Engineering Research Board of India and a grant from the Infosys Foundation. K.G.A. acknowledges support from the Department of Science and Technology and the Science and Engineering Research Board (SERB) of India via the following grants: Swarnajayanti Fellowship Grant DST/SJF/PSA-01/2017-18 and MATRICS grant (Mathematical Research Impact Centric Support) MTR/2020/000177. D.C. is supported by the STFC grant ST/V005618/1. D.C. and B.S.S. thank the Aspen Center for Physics (ACP) summer workshop 2022 for setting up discussions that also contributed to this collaborative work. F.A. is supported by the STFC Rutherford fellowship (ST/P00492X/2). K.G.A. and B.S.S. acknowledge the support of the Indo-US Science and Technology Forum through the Indo-US Centre for Gravitational-Physics and Astronomy, grant IUSSTF/JC-142/2019. We also acknowledge National Science Foundation (NSF) support via NSF awards AST-2205920 and PHY-2308887 to A.G., NSF CAREER award PHY-1653374 to M.F., and AST-2307147, PHY-2207638, PHY-2308886, and PHY-2309064 to B.S.S. The authors are grateful for computational resources provided by the Cardiff University and supported by STFC grants ST/I006285/1 and ST/V005618/1. This manuscript has the LIGO preprint number P2400227.

This research has made use of data obtained from the Gravitational Wave Open Science Center (<https://www.gwosc.org/>), a service of the LIGO Laboratory, the LIGO Scientific Collaboration and the Virgo Collaboration. LIGO Laboratory and Advanced LIGO are funded by the United States National Science Foundation (NSF) as well as the Science and Technology Facilities Council (STFC) of the United Kingdom, the

Max-Planck-Society (MPS), and the State of Niedersachsen/Germany for support of the construction of Advanced LIGO and construction and operation of the GEO600 detector. Additional support for Advanced LIGO was provided by the Australian Research Council. Virgo is funded, through the European Gravitational Observatory (EGO), by the French Centre National de Recherche Scientifique (CNRS), the Italian Istituto Nazionale di Fisica Nucleare (INFN) and the Dutch Nikhef, with contributions by institutions from Belgium, Germany, Greece, Hungary, Ireland, Japan, Monaco, Poland, Portugal, Spain. The construction and operation of KAGRA are funded by Ministry of Education, Culture, Sports, Science and Technology (MEXT), and Japan Society for the Promotion of Science (JSPS), National Research Foundation (NRF) and Ministry of Science and ICT (MSIT) in Korea, Academia Sinica (AS) and the Ministry of Science and Technology (MoST) in Taiwan.

APPENDIX

A. DETAILED RESULTS FROM INJECTION STUDIES

In this appendix, we present the detailed results from the injection studies described in Section 4. Tables 2 and 3 are aimed at exploring the parameter space of the parent black holes in binaries. Tables 4 and 5 present the recovery precision for various injection parameters assuming two different cluster metallicities. Figures 6 and 7 show the recovery of one hierarchical merger tree in two different clusters with different metallicities.

No.	$m_{1,p} (M_\odot)$		$m_{2,p} (M_\odot)$		$\chi_{1,p}$	$\chi_{2,p}$	$\theta_{1,p}$	$\theta_{2,p}$	$\phi_{12,p}$	$\chi_{\text{eff},p}$		$\chi_{p,p}$		$V_{\text{kick},p} \text{ (km/s)}$	
	Inj.	Rec.	Inj.	Rec.	Inj.	Inj.	Inj.	Inj.	Inj.	Inj.	Rec.	Inj.	Rec.	Inj.	Rec.
1	30	28_{-05}^{+09}	15	17_{-10}^{+05}	0.5	0.3	0.94	0.99	5.97	0.25	$0.12_{-0.29}^{+0.31}$	0.40	$0.49_{-0.36}^{+0.41}$	809	685_{-569}^{+1300}
2	40	39_{-08}^{+12}	20	21_{-13}^{+08}	0.5	0.3	1.62	1.23	1.42	0.02	$0.00_{-0.30}^{+0.30}$	0.50	$0.43_{-0.33}^{+0.44}$	1081	489_{-378}^{+982}
3	60	62_{-15}^{+18}	30	28_{-19}^{+15}	0.5	0.3	1.87	2.35	4.99	-0.17	$-0.06_{-0.32}^{+0.30}$	0.48	$0.40_{-0.31}^{+0.42}$	432	406_{-301}^{+773}
4	40	40_{-09}^{+12}	20	20_{-12}^{+09}	0.2	0.1	1.81	1.65	0.00	-0.03	$-0.04_{-0.30}^{+0.29}$	0.19	$0.40_{-0.31}^{+0.44}$	349	429_{-321}^{+870}
5	40	39_{-08}^{+12}	20	21_{-14}^{+08}	0.5	0.4	1.51	2.48	1.88	-0.09	$-0.01_{-0.30}^{+0.29}$	0.50	$0.42_{-0.32}^{+0.44}$	744	459_{-348}^{+956}
6	40	39_{-08}^{+12}	20	21_{-13}^{+08}	0.7	0.6	1.83	1.87	5.41	-0.18	$-0.02_{-0.30}^{+0.28}$	0.68	$0.42_{-0.33}^{+0.43}$	754	461_{-351}^{+891}
7	75	73_{-14}^{+12}	15	18_{-11}^{+16}	0.2	0.1	1.48	1.10	1.85	0.02	$-0.13_{-0.43}^{+0.27}$	0.20	$0.32_{-0.26}^{+0.34}$	193	261_{-196}^{+422}
8	75	76_{-13}^{+10}	15	14_{-07}^{+13}	0.5	0.4	2.14	2.10	1.43	-0.26	$-0.13_{-0.46}^{+0.23}$	0.42	$0.27_{-0.22}^{+0.29}$	313	178_{-130}^{+343}
9	75	80_{-10}^{+08}	15	09_{-04}^{+10}	0.7	0.6	2.91	1.93	5.36	-0.60	$-0.30_{-0.40}^{+0.22}$	0.16	$0.12_{-0.08}^{+0.07}$	236	115_{-82}^{+228}

Table 2. Summary of results from the simulated injection study that uses both mass and spin information of the hierarchical candidate BH. The injected values (Inj.) of the masses, spin parameters, and kick speeds of the simulated parent binaries are listed. We have drawn the mock posteriors for the mass and spin of the hierarchical candidate BH from the mass and spin of the remnant of the parent BBH assuming a Gaussian distribution. The means of the Gaussian distributions are the injected values of the remnant masses and spins, with the standard deviations taken to be 5% and 10% of the injected values (for the remnant masses and spins, respectively). The 90% credible intervals of the recovered posteriors (Rec.) on the masses, spin parameters, and kick speed of the parent binaries are also listed. The injected values of different parameters of the parent binaries are recovered well within 90% credibility.

No.	$m_{1,p}$ (M_\odot)		$m_{2,p}$ (M_\odot)		$\chi_{1,p}$	$\chi_{2,p}$	$\theta_{1,p}$	$\theta_{2,p}$	$\phi_{12,p}$	$\chi_{\text{eff},p}$		$\chi_{p,p}$		$V_{\text{kick},p}$ (km/s)	
	Inj.	Rec.	Inj.	Rec.	Inj.	Inj.	Inj.	Inj.	Inj.	Inj.	Rec.	Inj.	Rec.	Inj.	Rec.
1	30	31_{-08}^{+08}	15	14_{-08}^{+08}	0.5	0.3	1.26	2.56	2.75	0.02	$0.00_{-0.42}^{+0.45}$	0.48	$0.41_{-0.33}^{+0.43}$	774	462_{-353}^{+1229}
2	40	42_{-11}^{+11}	20	18_{-11}^{+12}	0.5	0.3	1.60	2.15	5.11	-0.06	$0.00_{-0.45}^{+0.45}$	0.50	$0.40_{-0.33}^{+0.45}$	537	425_{-334}^{+1216}
3	60	64_{-17}^{+17}	30	26_{-18}^{+18}	0.5	0.3	0.98	1.61	0.42	0.18	$0.00_{-0.44}^{+0.44}$	0.42	$0.40_{-0.32}^{+0.45}$	864	381_{-312}^{+1197}
4	40	42_{-11}^{+11}	20	18_{-11}^{+12}	0.2	0.1	1.49	0.67	1.51	0.04	$0.01_{-0.44}^{+0.43}$	0.20	$0.40_{-0.32}^{+0.46}$	418	412_{-325}^{+1223}
5	40	41_{-11}^{+11}	20	18_{-12}^{+11}	0.5	0.4	0.76	1.06	4.01	0.31	$0.00_{-0.45}^{+0.44}$	0.34	$0.40_{-0.33}^{+0.45}$	901	405_{-314}^{+1290}
6	40	42_{-11}^{+11}	20	18_{-12}^{+11}	0.7	0.6	1.21	1.55	1.16	0.17	$0.00_{-0.43}^{+0.44}$	0.65	$0.40_{-0.32}^{+0.45}$	1659	431_{-342}^{+1193}
7	75	65_{-17}^{+18}	15	26_{-19}^{+18}	0.2	0.1	1.09	0.77	1.11	0.09	$0.00_{-0.45}^{+0.46}$	0.18	$0.40_{-0.32}^{+0.46}$	178	396_{-328}^{+1226}
8	75	65_{-17}^{+18}	15	26_{-19}^{+18}	0.5	0.4	1.46	0.67	4.77	0.10	$0.00_{-0.45}^{+0.45}$	0.50	$0.39_{-0.32}^{+0.46}$	398	386_{-320}^{+1238}
9	75	67_{-17}^{+18}	15	26_{-19}^{+19}	0.7	0.6	2.11	0.38	2.72	-0.21	$0.00_{-0.43}^{+0.45}$	0.60	$0.41_{-0.33}^{+0.44}$	490	388_{-318}^{+1187}

Table 3. Summary of results from the simulated injection study that only uses the mass information of the hierarchical candidate BH. The columns are the same as in Table 2. Although the injected values of different parameters of the parent binaries are recovered within 90% credibility, the median values of the posteriors are slightly offset from the injected values for some cases.

No.	1g+2g										1g+1g									
	$m_{1,p}$		$m_{2,p}$		$\chi_{\text{eff},p}$		$\chi_{p,p}$		$V_{\text{kick},p}$		$m_{1,gp}$		$m_{2,gp}$		$\chi_{\text{eff},gp}$		$\chi_{p,gp}$		$V_{\text{kick},gp}$	
	Inj.	Rec.	Inj.	Rec.	Inj.	Rec.	Inj.	Rec.	Inj.	Rec.	Inj.	Rec.	Inj.	Rec.	Inj.	Rec.	Inj.	Rec.	Inj.	Rec.
1	52	49_{-11}^{+17}	23	26_{-19}^{+11}	0.44	$0.28_{-0.33}^{+0.34}$	0.43	$0.57_{-0.38}^{+0.42}$	168	819_{-696}^{+1407}	36	37_{-12}^{+17}	19	16_{-10}^{+13}	0.12	$0.00_{-0.44}^{+0.44}$	0.69	$0.41_{-0.32}^{+0.49}$	165	427_{-330}^{+1262}
2	73	69_{-15}^{+25}	33	37_{-28}^{+16}	0.37	$0.24_{-0.34}^{+0.34}$	0.61	$0.57_{-0.39}^{+0.42}$	64	774_{-678}^{+1410}	42	53_{-18}^{+26}	34	22_{-15}^{+19}	-0.06	$0.00_{-0.44}^{+0.44}$	0.87	$0.41_{-0.32}^{+0.49}$	226	409_{-333}^{+1254}
3	63	67_{-15}^{+22}	39	35_{-25}^{+15}	-0.22	$-0.02_{-0.31}^{+0.30}$	0.70	$0.43_{-0.38}^{+0.47}$	181	429_{-331}^{+938}	38	51_{-16}^{+24}	29	21_{-14}^{+18}	0.15	$0.01_{-0.43}^{+0.43}$	0.20	$0.42_{-0.33}^{+0.48}$	319	412_{-331}^{+1234}
4	71	67_{-14}^{+22}	33	37_{-28}^{+14}	0.34	$0.18_{-0.32}^{+0.34}$	0.27	$0.55_{-0.38}^{+0.43}$	392	717_{-619}^{+1381}	40	50_{-17}^{+25}	34	21_{-14}^{+19}	-0.44	$0.00_{-0.45}^{+0.45}$	0.16	$0.41_{-0.32}^{+0.49}$	165	410_{-330}^{+1222}
5	51	51_{-10}^{+19}	29	30_{-20}^{+10}	0.00	$0.05_{-0.30}^{+0.32}$	0.63	$0.48_{-0.36}^{+0.46}$	211	556_{-452}^{+1124}	36	38_{-12}^{+18}	17	16_{-10}^{+13}	0.00	$0.01_{-0.44}^{+0.43}$	0.12	$0.42_{-0.33}^{+0.49}$	206	431_{-331}^{+1233}
6	61	60_{-11}^{+08}	11	13_{-7}^{+12}	-0.30	$-0.13_{-0.45}^{+0.25}$	0.54	$0.28_{-0.23}^{+0.33}$	327	234_{-166}^{+359}	42	43_{-12}^{+14}	22	19_{-12}^{+13}	-0.09	$0.01_{-0.44}^{+0.43}$	0.28	$0.42_{-0.34}^{+0.48}$	350	423_{-337}^{+1268}
7	58	60_{-13}^{+21}	34	32_{-24}^{+14}	0.44	$0.26_{-0.35}^{+0.34}$	0.51	$0.57_{-0.39}^{+0.43}$	200	804_{-696}^{+1392}	35	45_{-15}^{+22}	26	19_{-12}^{+17}	0.10	$0.01_{-0.44}^{+0.45}$	0.17	$0.42_{-0.33}^{+0.48}$	341	424_{-341}^{+1246}
8	67	69_{-14}^{+27}	42	40_{-30}^{+14}	0.04	$0.11_{-0.31}^{+0.33}$	0.76	$0.51_{-0.37}^{+0.45}$	378	617_{-521}^{+1281}	41	52_{-17}^{+27}	29	22_{-15}^{+19}	-0.29	$0.00_{-0.44}^{+0.45}$	0.26	$0.42_{-0.34}^{+0.47}$	275	411_{-333}^{+1235}
9	63	64_{-15}^{+19}	30	29_{-20}^{+16}	-0.26	$-0.05_{-0.33}^{+0.29}$	0.69	$0.39_{-0.30}^{+0.46}$	364	395_{-295}^{+793}	41	48_{-16}^{+21}	25	19_{-13}^{+17}	0.00	$0.01_{-0.45}^{+0.45}$	0.24	$0.41_{-0.32}^{+0.49}$	276	411_{-331}^{+1286}
10	54	54_{-13}^{+17}	28	27_{-19}^{+13}	0.73	$0.32_{-0.35}^{+0.33}$	0.25	$0.58_{-0.39}^{+0.42}$	214	853_{-741}^{+1414}	30	40_{-13}^{+18}	26	17_{-11}^{+14}	-0.04	$0.01_{-0.44}^{+0.44}$	0.39	$0.42_{-0.33}^{+0.48}$	198	436_{-342}^{+1272}

Table 4. Summary of results from a simulated injection study of a few 1g+3g-merger chains from Mahapatra et al. (2022), assuming a cluster with metallicity $Z = 0.00015$ and escape speed $V_{\text{esc}} = 400$ km/s. The injected values (Inj.) of the masses, spin parameters, and kick speeds of the simulated parent (i.e., 1g+2g) and grandparent (i.e., 1g+1g) binaries are shown. We have drawn the mock posteriors for the remnant masses and spins for the parent binaries (i.e., the masses and spins of the 3g BHs, the remnant masses and spins of the 1g+2g binaries) from Gaussian distributions. The means of the Gaussians are the injected values of the remnant masses and spins; the standard deviations are taken to be 5% and 10% of the injected values of the remnant masses and spins, respectively. The 90% credible intervals of the recovered posteriors (Rec.) on the masses, spin parameters, and kick speeds of the parent and the grandparent binaries are reported. The injected values of different parameters of the parent and the grandparent binaries are recovered within 90% credibility.

Injected 1g+3g Chain

Recovered 1g+3g Chain

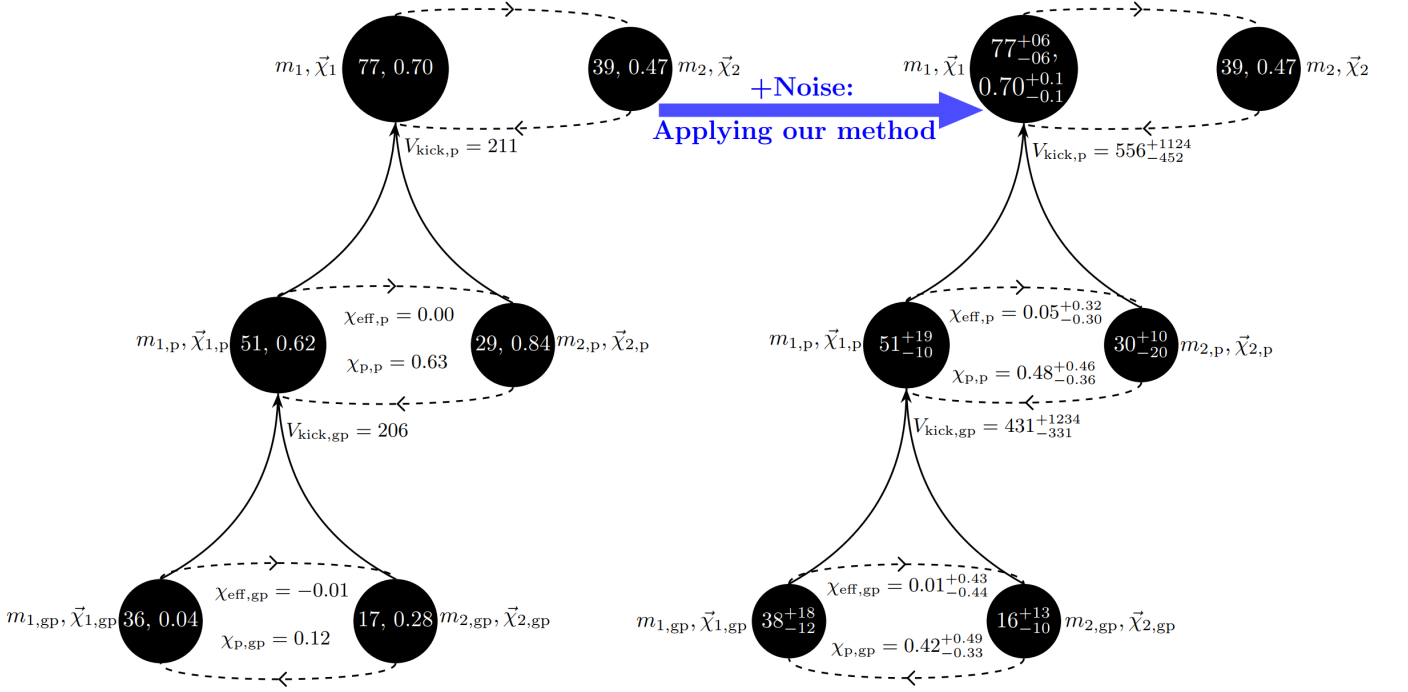


Figure 6. Injection and recovery of a mock 1g+3g chain in a cluster with escape speed $V_{\text{esc}} = 400$ km/s and metallicity $Z = 0.00015$. The left diagram depicts the injected 1g+3g merger chain, showing the (in principle) observed binary at top, the parent binary below, and the grandparent binary at bottom. Given the parameters of the grandparent binary, the mass, spin, and kick values of the later generations are consistent with the predictions of NR simulations. Gaussian noise is then added to the mass and spin parameters of the 3g (top) binary. Application of the Bayesian inference method described in Section 2 then allows a recovery of the merger history, as illustrated in the right part of the diagram. There, the numbers represent the 90% credible intervals on the inferred posterior distributions.

No.	1g+2g										1g+1g									
	$m_{1,p}$		$m_{2,p}$		$\chi_{\text{eff},p}$		$\chi_{p,p}$		$V_{\text{kick},p}$		$m_{1,gp}$		$m_{2,gp}$		$\chi_{\text{eff},gp}$		$\chi_{p,gp}$		$V_{\text{kick},gp}$	
	Inj.	Rec.	Inj.	Rec.	Inj.	Rec.	Inj.	Rec.	Inj.	Rec.	Inj.	Rec.	Inj.	Rec.	Inj.	Rec.	Inj.	Rec.	Inj.	Rec.
1	19	20^{+03}_{-04}	07	07^{+04}_{-01}	-0.26	$-0.24^{+0.27}_{-0.33}$	0.36	$0.32^{+0.37}_{-0.24}$	373	354^{+372}_{-187}	12	13^{+04}_{-03}	08	08^{+03}_{-02}	-0.19	$0.00^{+0.41}_{-0.41}$	0.31	$0.45^{+0.51}_{-0.33}$	316	546^{+1328}_{-411}
2	13	15^{+02}_{-03}	08	06^{+03}_{-01}	-0.46	$-0.25^{+0.27}_{-0.30}$	0.27	$0.34^{+0.39}_{-0.25}$	296	388^{+482}_{-210}	08	09^{+02}_{-02}	06	06^{+02}_{-01}	-0.03	$0.01^{+0.40}_{-0.40}$	0.26	$0.46^{+0.51}_{-0.34}$	340	569^{+1379}_{-447}
3	19	20^{+03}_{-04}	08	06^{+04}_{-01}	-0.35	$-0.27^{+0.28}_{-0.33}$	0.36	$0.32^{+0.33}_{-0.24}$	301	350^{+304}_{-183}	12	14^{+04}_{-03}	07	08^{+03}_{-03}	0.00	$0.00^{+0.43}_{-0.41}$	0.17	$0.44^{+0.49}_{-0.33}$	251	534^{+1382}_{-404}
4	16	16^{+02}_{-02}	06	06^{+02}_{-01}	-0.50	$-0.46^{+0.23}_{-0.23}$	0.32	$0.34^{+0.23}_{-0.21}$	363	365^{+209}_{-116}	09	10^{+02}_{-02}	07	07^{+02}_{-02}	0.06	$0.00^{+0.41}_{-0.41}$	0.44	$0.46^{+0.51}_{-0.34}$	270	550^{+1344}_{-431}
5	18	19^{+05}_{-04}	12	11^{+04}_{-05}	-0.18	$-0.01^{+0.28}_{-0.28}$	0.71	$0.42^{+0.50}_{-0.32}$	297	511^{+992}_{-387}	12	13^{+05}_{-03}	06	08^{+04}_{-02}	0.01	$0.00^{+0.42}_{-0.41}$	0.10	$0.44^{+0.51}_{-0.33}$	193	544^{+1373}_{-408}
6	17	19^{+02}_{-03}	08	06^{+02}_{-01}	-0.56	$-0.41^{+0.25}_{-0.25}$	0.17	$0.33^{+0.25}_{-0.22}$	336	354^{+204}_{-137}	11	12^{+03}_{-02}	07	07^{+02}_{-02}	0.00	$0.00^{+0.42}_{-0.41}$	0.20	$0.45^{+0.51}_{-0.33}$	366	549^{+1362}_{-415}
7	15	13^{+03}_{-02}	07	09^{+02}_{-03}	0.66	$0.26^{+0.32}_{-0.32}$	0.42	$0.55^{+0.49}_{-0.36}$	241	991^{+1379}_{-847}	08	09^{+03}_{-02}	07	06^{+02}_{-01}	-0.13	$0.01^{+0.40}_{-0.40}$	0.40	$0.47^{+0.54}_{-0.34}$	320	552^{+1338}_{-442}
8	17	18^{+05}_{-03}	12	11^{+03}_{-05}	-0.06	$0.07^{+0.30}_{-0.28}$	0.89	$0.48^{+0.47}_{-0.35}$	391	655^{+1214}_{-531}	12	12^{+05}_{-03}	06	07^{+03}_{-02}	-0.01	$0.01^{+0.41}_{-0.39}$	0.07	$0.44^{+0.50}_{-0.33}$	153	542^{+1388}_{-417}
9	19	19^{+02}_{-03}	07	06^{+02}_{-01}	-0.47	$-0.42^{+0.25}_{-0.24}$	0.33	$0.3^{+0.24}_{-0.21}$	344	348^{+187}_{-134}	12	13^{+03}_{-03}	07	08^{+03}_{-02}	-0.02	$0.00^{+0.43}_{-0.42}$	0.12	$0.44^{+0.50}_{-0.33}$	222	552^{+1405}_{-416}
10	15	14^{+03}_{-02}	08	09^{+03}_{-03}	-0.07	$0.03^{+0.27}_{-0.27}$	0.79	$0.44^{+0.52}_{-0.33}$	376	571^{+1160}_{-453}	09	09^{+03}_{-02}	07	06^{+18}_{-14}	0.15	$0.00^{+0.40}_{-0.41}$	0.29	$0.45^{+0.54}_{-0.33}$	284	538^{+1303}_{-428}

Table 5. Same as Table 4 except the 1g+3g-merger chains assume a cluster with metallicity $Z = 0.0225$ and escape speed $V_{\text{esc}} = 400$ km/s. We again find that the injected values of different parameters of the parent and the grandparent binaries are well recovered within 90% credibility.

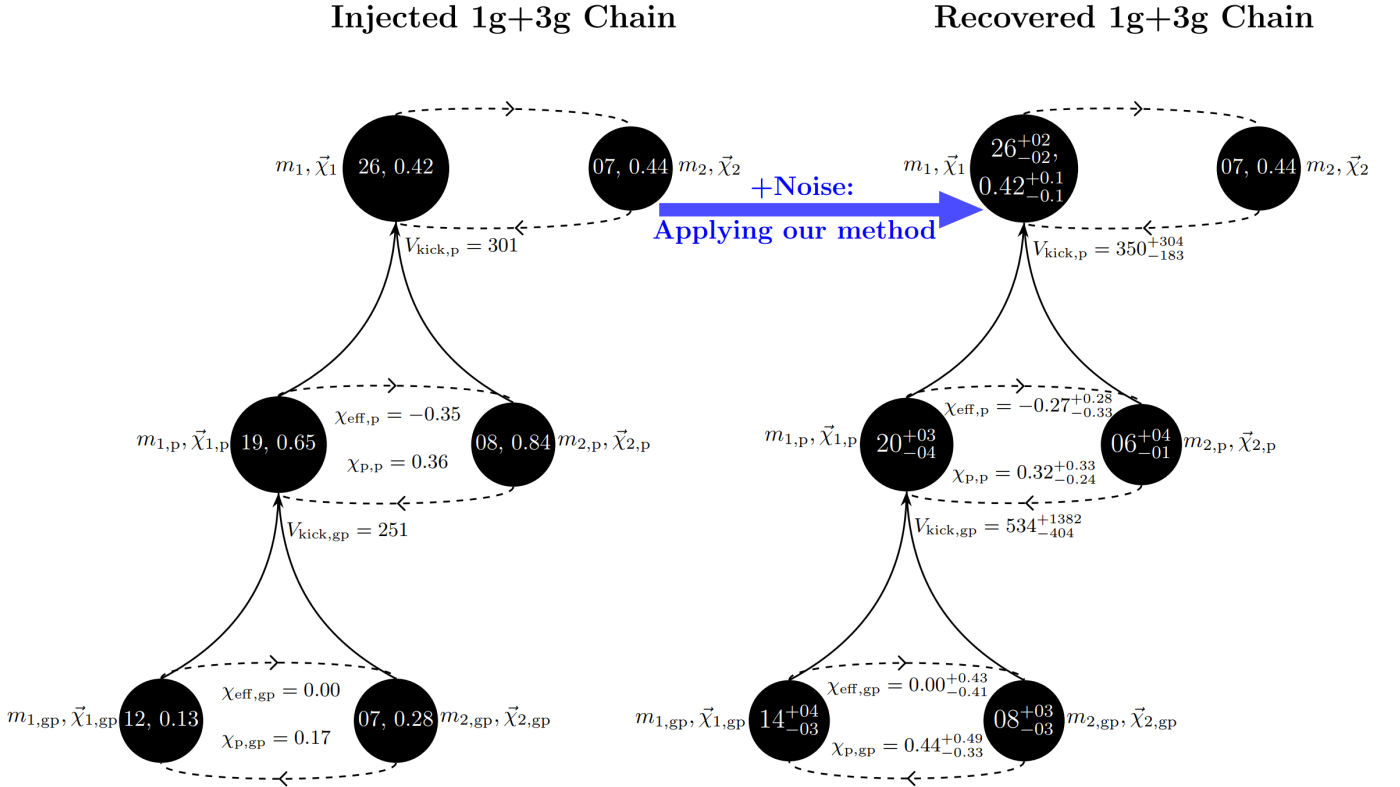


Figure 7. Same as Figure 6 except the 1g+3g chain is from a cluster with escape speed $V_{\text{esc}} = 400$ km/s and metallicity $Z = 0.0225$.

REFERENCES

- Aasi, J., et al. 2015, *Classical and Quantum Gravity*, 32, 074001, doi: [10.1088/0264-9381/32/7/074001](https://doi.org/10.1088/0264-9381/32/7/074001)
- Abbott, B. P., et al. 2017, *Classical Quantum Gravity*, 34, 044001, doi: [10.1088/1361-6382/aa51f4](https://doi.org/10.1088/1361-6382/aa51f4)
- . 2018, *Living Rev. Rel.*, 21, 3, doi: [10.1007/s41114-020-00026-9](https://doi.org/10.1007/s41114-020-00026-9)
- Abbott, R., et al. 2020a, *Phys. Rev. Lett.*, 125, 101102, doi: [10.1103/PhysRevLett.125.101102](https://doi.org/10.1103/PhysRevLett.125.101102)
- . 2020b, *Astrophys. J. Lett.*, 900, L13, doi: [10.3847/2041-8213/aba493](https://doi.org/10.3847/2041-8213/aba493)
- . 2020c, *Phys. Rev. D*, 102, 043015, doi: [10.1103/PhysRevD.102.043015](https://doi.org/10.1103/PhysRevD.102.043015)
- . 2020d, *Astrophys. J. Lett.*, 896, L44, doi: [10.3847/2041-8213/ab960f](https://doi.org/10.3847/2041-8213/ab960f)
- . 2021a, *Phys. Rev. X*, 11, 021053, doi: [10.1103/PhysRevX.11.021053](https://doi.org/10.1103/PhysRevX.11.021053)
- . 2021b, arXiv e-prints, arXiv:2111.03606, doi: [10.48550/arXiv.2111.03606](https://doi.org/10.48550/arXiv.2111.03606)
- . 2023a, *Phys. Rev. X*, 13, 011048, doi: [10.1103/PhysRevX.13.011048](https://doi.org/10.1103/PhysRevX.13.011048)
- . 2023b, *Phys. Rev. X*, 13, 041039, doi: [10.1103/PhysRevX.13.041039](https://doi.org/10.1103/PhysRevX.13.041039)
- . 2024, *Phys. Rev. D*, 109, 022001, doi: [10.1103/PhysRevD.109.022001](https://doi.org/10.1103/PhysRevD.109.022001)
- Acernese, F., Agathos, M., et al. 2014, *Classical and Quantum Gravity*, 32, 024001, doi: [10.1088/0264-9381/32/2/024001](https://doi.org/10.1088/0264-9381/32/2/024001)
- Antonini, F., Gieles, M., Dosopoulou, F., & Chattopadhyay, D. 2023, *Mon. Not. Roy. Astron. Soc.*, 522, 466, doi: [10.1093/mnras/stad972](https://doi.org/10.1093/mnras/stad972)
- Antonini, F., Gieles, M., & Gualandris, A. 2019, *Mon. Not. Roy. Astron. Soc.*, 486, 5008, doi: [10.1093/mnras/stz1149](https://doi.org/10.1093/mnras/stz1149)
- Antonini, F., & Rasio, F. A. 2016, *Astrophys. J.*, 831, 187, doi: [10.3847/0004-637X/831/2/187](https://doi.org/10.3847/0004-637X/831/2/187)
- Araújo-Álvarez, C., Wong, H. W. Y., & Bustillo, J. C. 2024. <https://arxiv.org/abs/2404.00720>
- Ashton, G., et al. 2019, *Astrophys. J. Suppl.*, 241, 27, doi: [10.3847/1538-4365/ab06fc](https://doi.org/10.3847/1538-4365/ab06fc)
- Baibhav, V., Berti, E., Gerosa, D., Mould, M., & Wong, K. W. K. 2021, *Phys. Rev. D*, 104, 084002, doi: [10.1103/PhysRevD.104.084002](https://doi.org/10.1103/PhysRevD.104.084002)
- Baker, J. G., Centrella, J., Choi, D.-I., Koppitz, M., & van Meter, J. 2006, *Phys. Rev. Lett.*, 96, 111102, doi: [10.1103/PhysRevLett.96.111102](https://doi.org/10.1103/PhysRevLett.96.111102)
- Banerjee, S. 2018, *Mon. Not. Roy. Astron. Soc.*, 473, 909, doi: [10.1093/mnras/stx2347](https://doi.org/10.1093/mnras/stx2347)
- Barausse, E., Morozova, V., & Rezzolla, L. 2012, *Astrophys. J.*, 758, 63, doi: [10.1088/0004-637X/758/1/63](https://doi.org/10.1088/0004-637X/758/1/63)
- Barausse, E., & Rezzolla, L. 2009, *ApJL*, 704, L40, doi: [10.1088/0004-637X/704/1/L40](https://doi.org/10.1088/0004-637X/704/1/L40)
- Barkat, Z., Rakavy, G., & Sack, N. 1967, *Phys. Rev. Lett.*, 18, 379, doi: [10.1103/PhysRevLett.18.379](https://doi.org/10.1103/PhysRevLett.18.379)
- Barrera, O., & Bartos, I. 2022, *Astrophys. J. Lett.*, 929, L1, doi: [10.3847/2041-8213/ac5f47](https://doi.org/10.3847/2041-8213/ac5f47)
- . 2024, *Astropart. Phys.*, 156, 102919, doi: [10.1016/j.astropartphys.2023.102919](https://doi.org/10.1016/j.astropartphys.2023.102919)
- Baxter, E. J., Croon, D., McDermott, S. D., & Sakstein, J. 2021, *Astrophys. J. Lett.*, 916, L16, doi: [10.3847/2041-8213/ac11fc](https://doi.org/10.3847/2041-8213/ac11fc)
- Britt, D., Johanson, B., Wood, L., Miller, M. C., & Michaely, E. 2021, *Mon. Not. Roy. Astron. Soc.*, 505, 3844, doi: [10.1093/mnras/stab1570](https://doi.org/10.1093/mnras/stab1570)
- Campanelli, M., Lousto, C. O., Marronetti, P., & Zlochower, Y. 2006, *Phys. Rev. Lett.*, 96, 111101, doi: [10.1103/PhysRevLett.96.111101](https://doi.org/10.1103/PhysRevLett.96.111101)
- Chandra, K., Pai, A., Leong, S. H. W., & Calderón Bustillo, J. 2024, *Phys. Rev. D*, 109, 104031, doi: [10.1103/PhysRevD.109.104031](https://doi.org/10.1103/PhysRevD.109.104031)
- Chattopadhyay, D., Hurley, J., Stevenson, S., & Raidani, A. 2022, *Mon. Not. Roy. Astron. Soc.*, 513, 4527, doi: [10.1093/mnras/stac1163](https://doi.org/10.1093/mnras/stac1163)
- Chattopadhyay, D., Stegmann, J., Antonini, F., Barber, J., & Romero-Shaw, I. M. 2023, *Mon. Not. Roy. Astron. Soc.*, 526, 4908, doi: [10.1093/mnras/stad3048](https://doi.org/10.1093/mnras/stad3048)
- Costa, G., Bressan, A., Mapelli, M., et al. 2021, *Mon. Not. Roy. Astron. Soc.*, 501, 4514, doi: [10.1093/mnras/staa3916](https://doi.org/10.1093/mnras/staa3916)
- Damour, T. 2001, *Phys. Rev. D*, 64, 124013, doi: [10.1103/PhysRevD.64.124013](https://doi.org/10.1103/PhysRevD.64.124013)
- Di Carlo, U. N., Mapelli, M., Bouffanais, Y., et al. 2020, *Mon. Not. Roy. Astron. Soc.*, 497, 1043, doi: [10.1093/mnras/staa1997](https://doi.org/10.1093/mnras/staa1997)
- Doctor, Z., Farr, B., & Holz, D. E. 2021, *Astrophys. J. Lett.*, 914, L18, doi: [10.3847/2041-8213/ac0334](https://doi.org/10.3847/2041-8213/ac0334)
- Farmer, R., Renzo, M., de Mink, S., Fishbach, M., & Justham, S. 2020, *Astrophys. J. Lett.*, 902, L36, doi: [10.3847/2041-8213/abbadd](https://doi.org/10.3847/2041-8213/abbadd)
- Farmer, R., Renzo, M., de Mink, S. E., Marchant, P., & Justham, S. 2019, *ApJ*, 887, 53, doi: [10.3847/1538-4357/ab518b](https://doi.org/10.3847/1538-4357/ab518b)
- Farrell, E. J., Groh, J. H., Hirschi, R., et al. 2021, *Mon. Not. Roy. Astron. Soc.*, 502, L40, doi: [10.1093/mnras/slaa196](https://doi.org/10.1093/mnras/slaa196)
- Favata, M., Hughes, S. A., & Holz, D. E. 2004, *Astrophys. J. Lett.*, 607, L5, doi: [10.1086/421552](https://doi.org/10.1086/421552)
- Fishbach, M., & Holz, D. E. 2020, *Astrophys. J. Lett.*, 904, L26, doi: [10.3847/2041-8213/abc827](https://doi.org/10.3847/2041-8213/abc827)

- Fishbach, M., Holz, D. E., & Farr, B. 2017, *Astrophys. J. Lett.*, 840, L24, doi: [10.3847/2041-8213/aa7045](https://doi.org/10.3847/2041-8213/aa7045)
- Fishbach, M., Kimball, C., & Kalogera, V. 2022, *Astrophys. J. Lett.*, 935, L26, doi: [10.3847/2041-8213/ac86c4](https://doi.org/10.3847/2041-8213/ac86c4)
- Fitchett, M. J. 1983, *Mon. Not. R. Astron. Soc.*, 203, 1049
- Fowler, W. A., & Hoyle, F. 1964, *Astrophys. J. Suppl.*, 9, 201, doi: [10.1086/190103](https://doi.org/10.1086/190103)
- Fragione, G., Ginsburg, I., & Kocsis, B. 2018, *Astrophys. J.*, 856, 92, doi: [10.3847/1538-4357/aab368](https://doi.org/10.3847/1538-4357/aab368)
- Fragione, G., & Rasio, F. A. 2023, *Astrophys. J.*, 951, 129, doi: [10.3847/1538-4357/acd9c9](https://doi.org/10.3847/1538-4357/acd9c9)
- Fragione, G., & Silk, J. 2020, *Mon. Not. Roy. Astron. Soc.*, 498, 4591, doi: [10.1093/mnras/staa2629](https://doi.org/10.1093/mnras/staa2629)
- Gayathri, V., Healy, J., Lange, J., et al. 2022, *Nature Astron.*, 6, 344, doi: [10.1038/s41550-021-01568-w](https://doi.org/10.1038/s41550-021-01568-w)
- Gerosa, D., & Berti, E. 2017, *Phys. Rev. D*, 95, 124046, doi: [10.1103/PhysRevD.95.124046](https://doi.org/10.1103/PhysRevD.95.124046)
- . 2019, *Phys. Rev. D*, 100, 041301, doi: [10.1103/PhysRevD.100.041301](https://doi.org/10.1103/PhysRevD.100.041301)
- Gerosa, D., & Fishbach, M. 2021, *Nature Astron.*, 5, 749, doi: [10.1038/s41550-021-01398-w](https://doi.org/10.1038/s41550-021-01398-w)
- Gerosa, D., Vitale, S., & Berti, E. 2020, *Phys. Rev. Lett.*, 125, 101103, doi: [10.1103/PhysRevLett.125.101103](https://doi.org/10.1103/PhysRevLett.125.101103)
- González, E., Kremer, K., Chatterjee, S., et al. 2021, *Astrophys. J. Lett.*, 908, L29, doi: [10.3847/2041-8213/abdf5b](https://doi.org/10.3847/2041-8213/abdf5b)
- Gupta, A., Gerosa, D., Arun, K. G., et al. 2020, *Phys. Rev. D*, 101, 103036, doi: [10.1103/PhysRevD.101.103036](https://doi.org/10.1103/PhysRevD.101.103036)
- Gupte, N., et al. 2024. <https://arxiv.org/abs/2404.14286>
- Healy, J., Lousto, C. O., & Zlochower, Y. 2014, *Phys. Rev. D*, 90, 104004, doi: [10.1103/PhysRevD.90.104004](https://doi.org/10.1103/PhysRevD.90.104004)
- Heger, A., Fryer, C. L., Woosley, S. E., Langer, N., & Hartmann, D. H. 2003, *Astrophys. J.*, 591, 288, doi: [10.1086/375341](https://doi.org/10.1086/375341)
- Hofmann, F., Barausse, E., & Rezzolla, L. 2016, *Astrophys. J. Lett.*, 825, L19, doi: [10.3847/2041-8205/825/2/L19](https://doi.org/10.3847/2041-8205/825/2/L19)
- Hurley, J. R., Pols, O. R., & Tout, C. A. 2000, *Mon. Not. Roy. Astron. Soc.*, 315, 543, doi: [10.1046/j.1365-8711.2000.03426.x](https://doi.org/10.1046/j.1365-8711.2000.03426.x)
- Kimball, C., Talbot, C., L. Berry, C. P., et al. 2020, *Astrophys. J.*, 900, 177, doi: [10.3847/1538-4357/aba518](https://doi.org/10.3847/1538-4357/aba518)
- Kimball, C., et al. 2021, *Astrophys. J. Lett.*, 915, L35, doi: [10.3847/2041-8213/ac0aef](https://doi.org/10.3847/2041-8213/ac0aef)
- Kinugawa, T., Nakamura, T., & Nakano, H. 2021, *Mon. Not. Roy. Astron. Soc.*, 501, L49, doi: [10.1093/mnras/slaa191](https://doi.org/10.1093/mnras/slaa191)
- Kremer, K., Spera, M., Becker, D., et al. 2020, *Astrophys. J.*, 903, 45, doi: [10.3847/1538-4357/abb945](https://doi.org/10.3847/1538-4357/abb945)
- Kritos, K., Stokov, V., Baibhav, V., & Berti, E. 2022. <https://arxiv.org/abs/2210.10055>
- Kroupa, P. 2001, *Mon. Not. Roy. Astron. Soc.*, 322, 231, doi: [10.1046/j.1365-8711.2001.04022.x](https://doi.org/10.1046/j.1365-8711.2001.04022.x)
- Lin, J. 1991, *IEEE Transactions on Information Theory*, 37, 145, doi: [10.1109/18.61115](https://doi.org/10.1109/18.61115)
- Liu, B., & Lai, D. 2021, *Mon. Not. Roy. Astron. Soc.*, 502, 2049, doi: [10.1093/mnras/stab178](https://doi.org/10.1093/mnras/stab178)
- Lousto, C. O., Campanelli, M., Zlochower, Y., & Nakano, H. 2010, *Class. Quant. Grav.*, 27, 114006, doi: [10.1088/0264-9381/27/11/114006](https://doi.org/10.1088/0264-9381/27/11/114006)
- Mahapatra, P., Gupta, A., Favata, M., Arun, K. G., & Sathyaprakash, B. S. 2021, *Astrophys. J. Lett.*, 918, L31, doi: [10.3847/2041-8213/ac20db](https://doi.org/10.3847/2041-8213/ac20db)
- . 2022. <https://arxiv.org/abs/2209.05766>
- Mapelli, M., et al. 2021, *Mon. Not. Roy. Astron. Soc.*, 505, 339, doi: [10.1093/mnras/stab1334](https://doi.org/10.1093/mnras/stab1334)
- Marchant, P., & Moriya, T. 2020, *Astron. Astrophys.*, 640, L18, doi: [10.1051/0004-6361/202038902](https://doi.org/10.1051/0004-6361/202038902)
- Marchant, P., Renzo, M., Farmer, R., et al. 2019, *ApJ*, 882, 36, doi: [10.3847/1538-4357/ab3426](https://doi.org/10.3847/1538-4357/ab3426)
- Merritt, D., Milosavljević, M., Favata, M., Hughes, S. A., & Holz, D. E. 2004, *Astrophys. J.*, 607, L9, doi: [10.1086/421551](https://doi.org/10.1086/421551)
- Miller, M. C., & Hamilton, D. P. 2002, *Mon. Not. Roy. Astron. Soc.*, 330, 232, doi: [10.1046/j.1365-8711.2002.05112.x](https://doi.org/10.1046/j.1365-8711.2002.05112.x)
- Mould, M., Gerosa, D., & Taylor, S. R. 2022, *Phys. Rev. D*, 106, 103013, doi: [10.1103/PhysRevD.106.103013](https://doi.org/10.1103/PhysRevD.106.103013)
- Natarajan, P. 2021, *Mon. Not. Roy. Astron. Soc.*, 501, 1413, doi: [10.1093/mnras/staa3724](https://doi.org/10.1093/mnras/staa3724)
- Nitz, A. H., & Capano, C. D. 2021, *Astrophys. J. Lett.*, 907, L9, doi: [10.3847/2041-8213/abcccc5](https://doi.org/10.3847/2041-8213/abcccc5)
- O’Leary, R. M., Rasio, F. A., Fregeau, J. M., Ivanova, N., & O’Shaughnessy, R. W. 2006, *Astrophys. J.*, 637, 937, doi: [10.1086/498446](https://doi.org/10.1086/498446)
- O’Shea, E., & Kumar, P. 2021. <https://arxiv.org/abs/2107.07981>
- Pretorius, F. 2005, *Phys. Rev. Lett.*, 95, 121101, doi: [10.1103/PhysRevLett.95.121101](https://doi.org/10.1103/PhysRevLett.95.121101)
- Racine, É. 2008, *Phys. Rev. D*, 78, 044021, doi: [10.1103/PhysRevD.78.044021](https://doi.org/10.1103/PhysRevD.78.044021)
- Reitze, D., et al. 2019, *Bull. Am. Astron. Soc.*, 51, 035. [https://arxiv.org/abs/arXiv:1907.04833\[astro-ph.IM\]](https://arxiv.org/abs/arXiv:1907.04833[astro-ph.IM)
- Renzo, M., Cantiello, M., Metzger, B. D., & Jiang, Y. F. 2020a, *Astrophys. J. Lett.*, 904, L13, doi: [10.3847/2041-8213/abc6a6](https://doi.org/10.3847/2041-8213/abc6a6)
- Renzo, M., Farmer, R., Justham, S., et al. 2020b, *Astron. Astrophys.*, 640, A56, doi: [10.1051/0004-6361/202037710](https://doi.org/10.1051/0004-6361/202037710)
- Renzo, M., Farmer, R. J., Justham, S., et al. 2020c, *Mon. Not. Roy. Astron. Soc.*, 493, 4333, doi: [10.1093/mnras/staa549](https://doi.org/10.1093/mnras/staa549)

- Rice, J. R., & Zhang, B. 2021, *Astrophys. J.*, 908, 59, doi: [10.3847/1538-4357/abd6ea](https://doi.org/10.3847/1538-4357/abd6ea)
- Rodriguez, C. L., Amaro-Seoane, P., Chatterjee, S., & Rasio, F. A. 2018, *Phys. Rev. Lett.*, 120, 151101, doi: [10.1103/PhysRevLett.120.151101](https://doi.org/10.1103/PhysRevLett.120.151101)
- Rodriguez, C. L., Zevin, M., Amaro-Seoane, P., et al. 2019, *Phys. Rev. D*, 100, 043027, doi: [10.1103/PhysRevD.100.043027](https://doi.org/10.1103/PhysRevD.100.043027)
- Rodriguez, C. L., et al. 2020, *Astrophys. J. Lett.*, 896, L10, doi: [10.3847/2041-8213/ab961d](https://doi.org/10.3847/2041-8213/ab961d)
- Romero-Shaw, I. M., Lasky, P. D., & Thrane, E. 2021, *Astrophys. J. Lett.*, 921, L31, doi: [10.3847/2041-8213/ac3138](https://doi.org/10.3847/2041-8213/ac3138)
- Romero-Shaw, I. M., Lasky, P. D., Thrane, E., & Bustillo, J. C. 2020, *Astrophys. J. Lett.*, 903, L5, doi: [10.3847/2041-8213/abbe26](https://doi.org/10.3847/2041-8213/abbe26)
- Roupas, Z., & Kazanas, D. 2019, *Astronomy & Astrophysics*, 632, L8, doi: [10.1051/0004-6361/201937002](https://doi.org/10.1051/0004-6361/201937002)
- Safarzadeh, M., & Haiman, Z. 2020, *Astrophys. J. Lett.*, 903, L21, doi: [10.3847/2041-8213/abc253](https://doi.org/10.3847/2041-8213/abc253)
- Salpeter, E. E. 1955, *ApJ*, 121, 161, doi: [10.1086/145971](https://doi.org/10.1086/145971)
- Sathyaprakash, B., Abernathy, M., Acernese, F., A., et al. 2012, *Class.Quant.Grav.*, 29, 124013. <https://arxiv.org/abs/1108.1423>
- Schmidt, P., Ohme, F., & Hannam, M. 2015, *Phys. Rev. D*, 91, 024043, doi: [10.1103/PhysRevD.91.024043](https://doi.org/10.1103/PhysRevD.91.024043)
- Skilling, J. 2004, in *American Institute of Physics Conference Series*, Vol. 735, *Bayesian Inference and Maximum Entropy Methods in Science and Engineering: 24th International Workshop on Bayesian Inference and Maximum Entropy Methods in Science and Engineering*, ed. R. Fischer, R. Preuss, & U. V. Toussaint, 395–405, doi: [10.1063/1.1835238](https://doi.org/10.1063/1.1835238)
- Speagle, J. S. 2020, *Mon. Not. Roy. Astron. Soc.*, 493, 3132, doi: [10.1093/mnras/staa278](https://doi.org/10.1093/mnras/staa278)
- Spera, M., & Mapelli, M. 2017, *Mon. Not. Roy. Astron. Soc.*, 470, 4739, doi: [10.1093/mnras/stx1576](https://doi.org/10.1093/mnras/stx1576)
- Tagawa, H., Haiman, Z., Bartos, I., & Kocsis, B. 2020, *Astrophys. J.*, 899, 26, doi: [10.3847/1538-4357/aba2cc](https://doi.org/10.3847/1538-4357/aba2cc)
- Tagawa, H., Kocsis, B., Haiman, Z., et al. 2021, *Astrophys. J.*, 908, 194, doi: [10.3847/1538-4357/abd555](https://doi.org/10.3847/1538-4357/abd555)
- Tanikawa, A., Susa, H., Yoshida, T., Trani, A. A., & Kinugawa, T. 2021, *Astrophys. J.*, 910, 30, doi: [10.3847/1538-4357/abe40d](https://doi.org/10.3847/1538-4357/abe40d)
- Tichy, W., & Marronetti, P. 2007, *Phys. Rev. D*, 76, 061502, doi: [10.1103/PhysRevD.76.061502](https://doi.org/10.1103/PhysRevD.76.061502)
- Tiwari, V., & Fairhurst, S. 2021, *Astrophys. J. Lett.*, 913, L19, doi: [10.3847/2041-8213/abfbc7](https://doi.org/10.3847/2041-8213/abfbc7)
- van Son, L. A. C., de Mink, S. E., Broekgaarden, F. S., et al. 2020, *Astrophys. J.*, 897, 100, doi: [10.3847/1538-4357/ab9809](https://doi.org/10.3847/1538-4357/ab9809)
- Varma, V., Field, S. E., Scheel, M. A., et al. 2019a, *Phys. Rev. Research.*, 1, 033015, doi: [10.1103/PhysRevResearch.1.033015](https://doi.org/10.1103/PhysRevResearch.1.033015)
- Varma, V., Gerosa, D., Stein, L. C., Hébert, F., & Zhang, H. 2019b, *Phys. Rev. Lett.*, 122, 011101, doi: [10.1103/PhysRevLett.122.011101](https://doi.org/10.1103/PhysRevLett.122.011101)
- Vink, J. S., de Koter, A., & Lamers, H. J. G. L. M. 2001, *Astron. Astrophys.*, 369, 574, doi: [10.1051/0004-6361:20010127](https://doi.org/10.1051/0004-6361:20010127)
- Woosley, S. E. 2017, *Astrophys. J.*, 836, 244, doi: [10.3847/1538-4357/836/2/244](https://doi.org/10.3847/1538-4357/836/2/244)
- Woosley, S. E., Blinnikov, S., & Heger, A. 2007, *Nature*, 450, 390, doi: [10.1038/nature06333](https://doi.org/10.1038/nature06333)
- Woosley, S. E., & Heger, A. 2021, *Astrophys. J. Lett.*, 912, L31, doi: [10.3847/2041-8213/abf2c4](https://doi.org/10.3847/2041-8213/abf2c4)
- Yang, Y., et al. 2019, *Phys. Rev. Lett.*, 123, 181101, doi: [10.1103/PhysRevLett.123.181101](https://doi.org/10.1103/PhysRevLett.123.181101)
- Zevin, M., & Holz, D. E. 2022, *Astrophys. J. Lett.*, 935, L20, doi: [10.3847/2041-8213/ac853d](https://doi.org/10.3847/2041-8213/ac853d)